Universidade Nova de Lisboa
Instituto de Higiene e Medicina Tropical

The role of the RhoGEF protein Solo in Src regulation in triple-negative breast cancer

Miguel Ângelo Ferreira

DISSERTAÇÃO PARA A OBTENÇÃO DO GRAU DE MESTRE EM CIÊNCIAS BIOMÉDICAS

Janeiro 2023

Universidade Nova de Lisboa
Instituto de Higiene e Medicina Tropical

University of Stuttgart
Institute of Cell Biology and Immunology

The role of the RhoGEF protein Solo in Src regulation in triple-negative breast cancer

Autor: Miguel Ângelo Ferreira

Orientador: Prof.ª Dr.ª Monilola Olayioye

Coorientador: Dr.ª Cristiana Lungu
MSc Florian Meyer

Dissertação apresentada para cumprimento dos requisitos necessários à obtenção do grau de Mestre em Ciências Biomédicas

Preface

The work presented in this thesis was performed at the *Institut für Zellbiologie und Immunologie* of the University of Stuttgart (Stuttgart, Germany) during the period October 2021 to July 2022, under the supervision of Prof. Dr. Monilola Olayioye, Dr. Cristiana Lungu and MSc Florian Meyer and within the frame of the Erasmus+ programme.

Acknowledgements

First of all, I would like to thank Prof. Dr. Monilola Olayioye for giving me the opportunity to work in this exciting project, for helping me through all the difficulties, for the scientific input, the constructive feedback and for the positive energy inside and outside the laboratory.

I would also like to express my gratitude to Dr. Cristiana Lungu for supervising my work, for giving me the opportunity to express my ideas, to encourage me to ask for help when needed and for teaching me how to be better organized and how to better manage my time and tasks. Additionally, I would also like to thank her for helping me integrate and adapt to the laboratory and for her friendship.

Furthermore, I would like to thank everyone at the Mo-Lab, especially those who shared a room-sized table with me, Stella, Kai, Yannick, Lisa, and Daniel. I have to thank Elena, Hazal, Merih and Sara as well for their friendship and for their great company during lunch. To the whole IZI, for their friendship, companionship and for teaching me not only how to be a better student/worker but also for teaching me about their cultures, languages, traditions, and points of view on all sorts of things. I would also like to recognize all the help from Dr. Stephan Eisler with the microscope. I am eternally grateful to have crossed paths with you all.

I especially would like to thank Florian Meyer, my supervisor, laboratory, and liquid nitrogen partner and, most of all, friend. I am extremely grateful to you for welcoming me, for your patience and self-control over my uncertainties and for teaching me everything that I needed to complete this thesis and more. Thank you for always being there for me through these complicated but exciting 10 months and for your really bad, but appreciated, jokes.

Por fim gostava de agradecer a todos os meus amigos pelo apoio que sempre me deram a nível pessoal e académico e também à minha família, em especial aos meus pais, por todos os esforços e sacrifícios que me permitiram ter tido o percurso académico que escolhi.

This page was intentionally left blank.

Resumo

O cancro da mama triplo-negativo (TNBC) é o mais agressivo subgrupo de cancro da mama (BC), associado a uma elevada chance de metastização. Para que a metastização possa ocorrer, migração celular é necessária. Este processo é dependente de adesões focais (FAs), cruciais para a ancoragem e para a comunicação da célula com a matriz extracelular (ECM), e do citoesqueleto de actina, que é fortemente regulado por Rho GTPases. A proteína RhoGEF Solo foi observada estar sobreexpressa em células TNBC e a sua depleção resultar numa diminuição em motilidade celular. Adicionalmente, Solo foi recentemente descoberta como sendo reguladora de RhoB em membranas endossomais em células HeLa. Além disto, RhoB está associada com o tráfego de proteínas sinalizadoras em endossomas entre a região peri-nuclear e a periferia celular. Uma destas proteínas é a quinase Src, uma das principais proteínas das FAs, frequentemente sobreexpressa em células TNBC. Curiosamente, dados do nosso laboratório revelaram Solo como sendo fosforilada por Src mas uma função não foi ainda identificada. Para além disto, o papel de Solo no tráfego de Src ainda não foi descrito.

O objetivo desta tese foi estudar os efeitos do *knock down* de Solo no tráfego de Src e no desenvolvimento de FAs por imunofluorescência. Para isto, as linhas celulares MDA-MB-231 e BT549 foram selecionadas enquanto sistemas modelo. Células shSolo MDA-MB-231estáveis induzidas por doxiciclina foram também geradas. Curiosamente, foi possível observar que ambos os *knock down* transiente e estável de Solo resultaram na acumulação de Src na região subcelular peri-nuclear e na redução da atividade de Src em células shSolo MDA-MB-231. Células shSolo apresentaram FAs mais longas e níveis de fosfotirosina reduzidos na periferia celular. Adicionalmente, os níveis de fosfotirosina do efetor *downstream* de Src, Paxilina, foi observado como estando diminuídos nas FAs, mesmo que um aumento global na fosforilação de Paxilina tenha sido quantificado. Numa matriz 3D, agrupamentos de células shSolo MDA-MB-231mostraram uma diminuição dos níveis de Src assim como menos Src extracelular. Em suma, estes resultados sugerem que Solo afeta o tráfego de Src entre as região peri-nuclear e a periferia celular.

No futuro, considerando que ambas as proteínas Solo e Src estão conectadas com endossomas RhoB-positivos, seria relevante identificar outras vias que poderão ser afetadas por este eixo. Adicionalmente, as linhas celulares BT549 e HS578T poderão ser usados como modelos para ensaios adicionais de forma a compreender se os efeitos observados nesta tese são conservados em diferentes linhas celulares de TNBC. Em resumo, detalhar a base subjacente do papel de Solo em TNBC é essencial para compreender o seu fenótipo agressivo e para o desenvolvimento de tratamentos futuros.

Palavras-chave: Cancro da mama; Rho GTPases; Solo; Src; Adesões focais.

Abstract

Triple-negative breast cancer (TNBC) is the most aggressive subgroup of breast cancer (BC), associated with an increased likelihood of metastasis. So that metastasis can occur, cell migration is necessary. This process is dependent on focal adhesions (FAs), that are crucial for cell anchorage and communication with the extracellular matrix (ECM), and the actin cytoskeleton, which is tightly regulated by Rho GTPases. The RhoGEF protein Solo was found to be overexpressed in TNBC cells and its depletion to result in decreased cell motility. Furthermore, Solo was also discovered to regulate RhoB at endosomal membranes in HeLa cells. RhoB is associated with endosomal trafficking of signaling proteins between the perinuclear region and the cell periphery. One of such proteins is the kinase Src, one of the main FA proteins, frequently overexpressed and overactive in TNBC cells. Interestingly, data from our lab revealed Solo to be phosphorylated by Src but a function has not yet been identified. Besides, the involvement of Solo in Src trafficking has not yet been described.

The aim of this thesis was to study the effects of Solo knock down on Src trafficking and FAs development by immunofluorescence. To this end, the MDA-MB-231 and BT549 cell lines were selected as model systems. Stable doxycycline-induced shSolo MDA-MB-231 cells were also generated. Strikingly, it could be shown that both transient and stable Solo knock down resulted in an accumulation of Src at the perinuclear subcellular region and decreased Src activity in shSolo MDA-MB-231 cells. shSolo cells showed longer FAs and decreased phosphotyrosine levels at the cell periphery. Additionally, the phosphorylation levels of the Src downstream effector Paxillin was also observed to be decreased at the FAs, even though an overall increase in Paxillin phosphorylation was quantified. In a 3D matrix, shSolo MDA-MB-231 cell spheroids showed a decrease in Src levels as well as less extracellular Src. Together, these results suggest that Solo affects Src trafficking in between the perinuclear region and the cell periphery.

For the future, as both Solo and Src are connected to RhoB-positive endosomes, it would be interesting to identify other pathways that could be affected by this axis. Additionally, BT549 and HS578T cell lines could be used as models in further experiments to understand if the effects observed in this thesis are conserved in different TNBC cell lines. In short, detailing the underlying basis of the role of Solo in TNBC is essential for understanding its aggressive phenotype and for the development of future treatments.

Keywords: Breast Cancer; Rho GTPases; Solo; Src; Focal adhesions.

Contents

Preface ..... **i**
Acknowledgements ..... **ii**
Resumo ..... **iv**
Abstract ..... **v**
List of figures and tables ..... **ix**
List of figures ix
List of tables x
Abbreviations ..... **xii**
1. Introduction 1
1.1 Breast cancer 1
1.2 Focal adhesions 2
1.3 Actin cytoskeleton 4
1.4 Rho GTPases 5
1.5 The RhoGEF Solo 8
1.6 The protooncogene Src 9
1.7 Src secreted in exosomes 11
1.8 Breast cancer cells in three-dimensions 11
1.9 Aims of this thesis 12
2. Materials 13
2.1 Chemicals, reagents, and solvents 13
2.2 Buffers and solutions 15
2.3 Cell culture 15
2.3.1 Cell culture reagents 15
2.3.2 Cell culture medium 16
2.3.3 Transfection reagents 16
2.4 Antibodies and dyes 17
2.4.1 Primary antibodies 17
2.4.2 Secondary antibodies 17
2.4.3 Dyes 17
2.5 Enzymes and Kits 18
2.5.1 Enzymes 18
2.5.2 Kits 18
2.6 Oligonucleotides 18
2.6.1 siRNAs 18

2.6.2 shRNAs 18
2.7 Plasmids 19
2.8 Cell lines 19
2.9 Equipment and consumables 20
2.9.1 Equipment 20
2.9.2 Consumables 21
2.10 Software 22
3. Methods 23
3.1 Cell culture 23
3.2 Transformation of *Escherichia coli*, plasmid amplification and isolation 24
3.3 Generation of stable cell lines 24
3.4 Puromycin titration 25
3.5 siRNA cell transfection 26
3.6 Cell lysis and protein concentration determination 26
3.7 SDS polyacrylamide gel electrophoresis (SDS-PAGE) 27
3.8 Western Blotting 27
3.9 3D cell culture 27
3.10 2D immunofluorescence 28
3.11 3D immunofluorescence 29
3.12 Statistical analysis 30
4. Results 31
4.1 Solo depleted MDA-MB-231 and BT549 cells showed increased Paxillin intensity at FAs 31
4.2 Solo knock down in MDA-MB-231 and BT549 cells lead to Src accumulation at the perinuclear region 34
4.3 Solo depleted MDA-MB-231 and BT549 cells showed an altered relative amount of phosphorylated Src and Paxillin 35
4.4 Stable shSolo cells were successfully generated 37
4.5 shSolo MDA-MB-231 cells showed decreased Src activity and increased levels of phosphorylated Paxillin 38
4.6 shSolo MDA-MB-231 cells showed decreased total Paxillin and Y118 phosphorylated Paxillin at the FAs 40
4.7 shSolo MDA-MB-231 cells showed an increase in perinuclear Src 42
4.8 Overall tyrosine residues were relatively less phosphorylated in FAs in shSolo MDA-MB-231 cells 43

4.9 Src showed a decrease intra and extracellularly in 3D spheroids for shSolo MDA-MB-231 cells 44
5. Discussion 47
5.1 Solo regulates Src localization and activity in stable MDA-MB-231 cells 47
5.2 Solo regulates Src downstream signaling 49
5.3 Src localization is affected by Solo depletion in 3D spheroids 52
5.4 Outlook 54
References 57

List of figures and tables

List of figures

Figure 1. Scheme of a focal adhesion. 3
Figure 2. Actin filaments in migrating cells. 5
Figure 3. The Rho GTPases cycle. 6
Figure 4. Src regulation. 10
Figure 5. Paxillin at focal adhesions is increased upon transient Solo knock down. 33
Figure 6. Src accumulates at the perinuclear region upon knock down of Solo in MDA-MB-231 cells. 35
Figure 7. Focal adhesion signaling is altered by transient knock down of Solo in MDA-MB-231 and BT549 cells. 36
Figure 8. Characterization of stable MDA-MB-231 cells with doxycycline-inducible shSolo expression. 38
Figure 9. Relative amount of phosphorylated Src decreases and phosphorylated Paxillin increases in stable shSolo MDA-MB-231 cells. 39
Figure 10. Paxillin and pPaxillin are reduced in stable shSolo MDA-MB-231 cells. 41
Figure 11. Src accumulates at the perinuclear region upon Solo knock down in stable cells. 42
Figure 12. Phosphotyrosines at focal adhesions are reduced in shSolo stable MDA-MB-231 cells. 44
Figure 13. Extracellular and total Src are decreased for shSolo MDA-MB-231 spheroids in 3D conditions. 46

List of tables

Table 1. Chemicals, reagents, and solvents used. 13
Table 2. Buffers and solutions used. 15
Table 3. Cell culture reagents used. 15
Table 4. Cell culture medium used. 16
Table 5. Transfection reagents used. 16
Table 6. Primary antibodies used. 17
Table 7. Secondary antibodies used. 17
Table 8. Dyes used. 17
Table 9. Enzymes used. 18
Table 10. Kits used. 18
Table 11. siRNAs used. 18
Table 12. shRNAs used. 18
Table 13. Plasmids used. 19
Table 14. Cell lines used. 19
Table 15. Equipment used. 20
Table 16. Consumables used. 21
Table 17. Software used. 22
Table 18. Transfection mix used for PEI transfection of LentiX 293T cells. 25
Table 19. Excitation wavelenghts and detection window used. 29

This page was intentionally left blank.

Abbreviations

2D	Two-dimensions
3D	Three-dimensions
a.u.	Arbitrary units
ACAFA	Actin cap associated focal adhesions
A-loop	Activation loop
ATP	Adenosine triphosphate
BC	Breast cancer
ddH2O	Double-distilled water
DH	Dbl-homology
DLC3	Deleted in liver cancer 3
DMEM	Dulbecco's Modified Eagle's Medium
DMSO	Dimethyl sulfoxide
DNA	Deoxyribonucleic acid
ECM	Extracellular matrix
EE	Early endosomes
EGF	Epidermal growth factor
EGFR	Epidermal growth factor receptor
EMT	Epithelial-to-mesenchymal transition
ER	Estrogen receptor
ERC	Endocytic recycling compartment
FA	Focal adhesion
FAK	Focal adhesion kinase
FCS	Fetal calf serum
FRAP	Fluorescence recovery after photobleaching
FX	Focal complex
GAP	GTPase-activating protein
GAPDH	Glyceraldehyde 3-phosphate dehydrogenase
GBD	GTPase-binding domain
GDI	Guanine nucleotide dissociated inhibitor
GDP	Guanosine diphosphate
GEF	Guanine nucleotide exchange factor
GTP	Guanosine triphosphate

HER2	Epidermal growth factor receptor 2
HUVEC	Human umbilical vein endothelial cells
IDR	Intrinsically disordered regions
K8/K18	Keratin-8/Keratin-18 filaments
LE	Late endosomes
LIM	Lin11, Isl-1, Mec-3
mDia2	Mammalian Diaphanous-related 2 formin
MFI	Mean fluorescence intensity
mRNA	Messenger RNA
mTNBC	Metastatic triple-negative breast cancer
NF-κB	Nuclear factor kappa-light-chain-enhancer of activated B cells
PABP1	Polyadenylation binding protein 1
PBS	Phosphate-buffered saline
PEI	Polyethyleneimine
PFA	Paraformaldehyde
PH	Pleckstrin homology
PR	Progesterone receptor
RBD	Rho-binding domain
rcf	Relative centrifugal force
RhoB-F	Farnesylated RhoB
RhoB-GG	Geranylgeranylated RhoB
ROCK	Rho-associated, coiled-coil containing protein kinase
rpm	Revolutions *per* minute
RT	Room temperature
RTK	Receptor tyrosine kinase
SDS-PAGE	Sodium dodecylsulfate polyacrylamide gel electrophoresis
SFK	Src-family kinase
SH1	Src-homology 1
SH2	Src-homology 2
SH3	Src-homology 3
SH4	Src-homology 4
shRNA	Short hairpin RNA
siRNA	Small interfering RNA
TIRF	Total internal reflection fluorescence microscopy
TNBC	Triple-negative breast cancer

1. Introduction

1.1 Breast cancer

Breast cancer (BC) is currently the most diagnosed type of cancer and the major cause of cancer-related death in women globally (Nedeljković 2019). In the year 2020 2.3 million women were diagnosed with BC and more than 600 thousand lives were lost due to this malignancy (WHO 2021). BC, however, is an extremely heterogeneous disease. This heterogeneity culminates onto a variety of molecular and prognostic profiles, translating into major therapeutic challenges (El Hachem *et al.* 2019). Within the spectrum of BC, tumors can be subdivided into different subgroups, based on the immunohistochemical expression of estrogen and progesterone receptors (ER and PR, respectively) and the Human Epidermal Growth Factor Receptor 2 (HER2) (Vagia et al. 2020). One of these subgroups is known as Triple-negative breast cancer (TNBC), being ER, PR and HER2 negative (Ullah 2019). TNBC, responsible for 15% to 20% of all breast cancers, is associated with a more aggressive course, as well as earlier recurrence and metastasis and developing more frequently in younger premenopausal women when compared to the other BC subgroups. Considering the limited treatment options and the aggressiveness of this BC subtype, it is vital that TNBC features are well understood, together with the discovery of potential therapeutic targets and the development of new therapeutic strategies. (Vagia *et al.* 2020, Sun *et al.* 2020).

In most cases of BC, the primary tumor is not the main cause of death, but the metastases at distant sites (Weigelt *et al.* 2005). Currently, chemotherapy is the most common systemic medical treatment for metastatic TNBC (mTNBC), but responses are frequently short-lived and patients have a median overall survival of 12 to 18 months (Keenan *et al.* 2020). That being the case, patients with mTNBC continue to have a significantly worse overall survival when compared to patients with other subgroup of metastatic BC (Zeichner *et al.* 2016). Metastasis is a process in which cell migration and colonization occurs in a multistep cascade of molecular events as a consequence of gene mutations and altered expression. Considering this, changes in cell phenotype are necessary (Khaled *et al.* 2019). For carcinomas to acquire an invasive behavior, it is imperative that a subgroup of cells undergo an epithelial-to-mesenchymal transition (EMT) (Lin *et al.*

2012). In EMT, cell-cell adhesions are lost and cytoskeleton alterations occur in order for cells to take on the properties of migratory mesenchymal cells (Ullah 2019).

1.2 Focal adhesions

During migration, large multi-protein structures serve as cell anchors and allow them to communicate with the extracellular matrix (ECM). These structures, known as focal adhesions (FAs), are dynamic structures that assemble, disassemble and mature at the extending leading edge of the cell and disassemble at the rear end for efficient migration (Deakin and Turner 2008). The molecular composition of FAs may vary considering the different intra- and extracellular inputs that they receive from their environment. These inputs, such as growth factors, result in the recruitment of more than 30 different adaptor proteins, providing binding platforms for hundreds of other intracellular FA proteins (Legerstee *et al.* 2021).

The process from which cells bind to external components has integrins as their main regulator, transmembrane αβ-integrin heterodimers serving as bridges between the ECM and the intracellular signaling machinery. Integrin cytoplasmic domains do not show intrinsic enzyme activity, but they allow for other intracellular proteins to dock to itself (Deakin and Turner 2008). A simplified scheme is represented in **Figure 1**. One of the main FA proteins is Paxillin (Xue *et al.* 2022), a scaffolding protein that contributes to the recruitment of specific kinases and phosphatases, cofactors, oncoproteins and structural proteins (López-Colomé *et al.* 2017). In addition to its FAs localization, Paxillin is known to be present in the cytoplasm and at nuclear regions (Hu *et al.* 2014). Considering its nuclear localization, Paxillin may also affect gene transcription, allowing a connection between the plasma membrane and cytoskeleton to the nucleus. For instance, Dong *et al.* demonstrated that in NIH-3T3 derived cell lines the expression of the H19 gene, suggested to promote tumorigenesis, was suppressed by nuclear Paxillin, thus confirming Paxillin to modulate the expression of H19 at the transcriptional level (Dong *et al.* 2009).

In a variety of cancers, the expression of Paxillin is known to be increased, as well as other FA proteins that interact with Paxillin, namely focal adhesion kinase (FAK) and the non-receptor tyrosine kinase Src. Paxillin is known to have an important role in matrix

organization, cell proliferation and survival, cell motility and cancer metastasis (Noh *et al.* 2020). Furthermore, this protein also coordinates the activation of RhoA, Rac1 and Cdc42 through the recruitment of guanine nucleotide exchange factors (GEFs) and GTPase-activating proteins (GAPs, see **1.4 Rho GTPases**) to FAs, allowing the activation of various cell migration-related pathways, ultimately resulting in the actin cytoskeleton reorganization (López-Colomé *et al.* 2017).

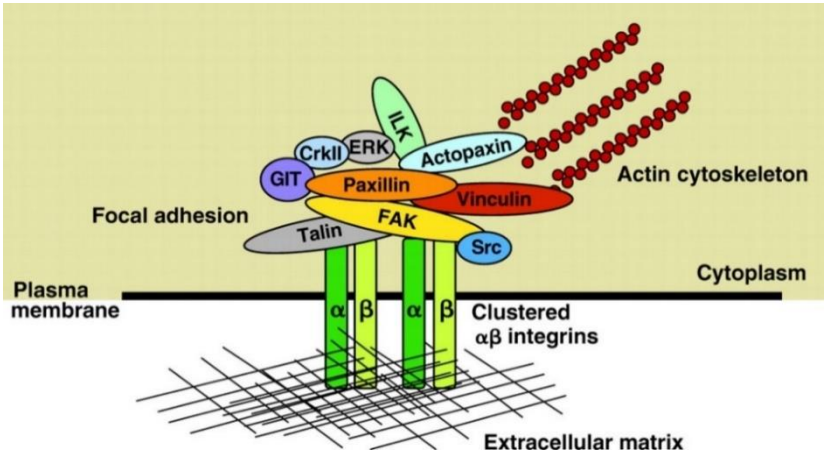

Figure 1. Scheme of a focal adhesion. Once a cell adheres to the ECM via transmembrane αβ-integrin heterodimers, various intracellular proteins are recruited to the plasma membrane, interacting with each other by virtue of the scaffolding protein Paxillin. The figure illustrates a simplified scheme, showing some of the main components of a FA (Deakin and Turner 2008).

The C-terminal of Paxillin contains four Lin11, Isl-1, Mec-3 (LIM) domains, LIM2 and LIM3 being necessary for targeting the protein to FAs, while the N-terminal domains of Paxillin control most of its signaling activity (Ma *et al.* 2018). This protein, by transmitting extracellular signals into the intracellular space, allows the activation of signaling cascades that are necessary for cell migration. As an example, cell adhesion and growth factor stimulation are able to activate FAK and Src. In turn, such kinases phosphorylate Paxillin, allowing for the recruitment of downstream molecules, such as CRK, leading to the modulation of gene expression and changes in cell motility (Turner 2000). As a result of the activation of such pathways, the cytoskeleton is reorganized and FAs are assembled/disassembled. During cell movement and migration Paxillin is recruited to nascent FAs at the cell front, being necessary for FAs turnover, that is, adhesion disassembly (Hu *et al.* 2014).

Paxillin is a target of multiple tyrosine kinases that are activated through the signaling of the αβ-integrins (Turner 2000). The function and localization of Paxillin is regulated by its phosphorylation, which can occur in multiple tyrosine and serine residues (Fu *et al.* 2021). Tyrosine phosphorylation is crucial for the FAs dynamics and cell migration control. However, the major phosphorylation site of this protein is Y118 (Qin *et al.* 2015), which promotes Paxillin disassembly from FAs, inducing cell migration (López-Colomé *et al.* 2017). Additionally, this process is known to occur in a FAK and Src-dependent manner (Shortrede *et al.* 2016). FAK, upon interaction with integrin, can be autophosphorylated at Y397. This generates a binding site for the Src-homology 2 domain (SH2) of Src, thus recruiting Src to FAs for the formation of the FAK/Scr kinase complex. This allows Src to phosphorylate FAK in several residues, leading to further FAK activation. Both Src and FAK activity are required for maximal tyrosine phosphorylation of Paxillin (Sachdev *et al.* 2009). As a scaffolding protein, the phosphorylation of Paxillin leads to the recruitment of proteins which, eventually, also contribute to the actin cytoskeleton regulation (López-Colomé *et al.* 2017).

1.3 Actin cytoskeleton

In order for individual cells to move, they extend their plasma membrane at the leading edge, move their body, and retract the tail of the cell. These membrane extensions, also known as protrusions, can be categorized in three different actin filament structures, lamellipodia, filopodia or stress fibers – representative scheme in **Figure 2** – each uniquely contributing to migration (Lehtimäki *et al.* 2021). Their formation is driven by the actin cytoskeleton, which is formed by actin molecules, actin filaments, actin-binding proteins, and regulatory proteins. This highly regulated filamentous network enables not only dynamic cell processes such as cell migration, intracellular trafficking or cell division, but provides structure as well (Ampe *et al.* 2016). In these processes, force is produced through actin filaments by two distinct mechanisms: actin polymerization of actin filaments against cellular membranes or, alternatively, the formation of contractile structures between actin filaments and myosin II filaments (Tojkander *et al.* 2012). In the first case, lamellipodia and filopodia have major roles in pulling the cell through the tissue by extending in long distances and exploring the cell's surroundings (Ridley 2011). In the latter case, the ATP-dependent movement of myosin II domains along the actin filaments

generates the necessary force for the contraction. The main contractile actomyosin structure in various mammalian cells are stress fibers, particularly common in various cancer cell lines, and being often coupled with FAs (Tojkander *et al.* 2012). Stress fibers have a major role in adhesion, mechanosensing, great contribution to cell morphogenesis and tail retraction during migration (Lehtimäki *et al.* 2021). Moreover, such actin structures are controlled by a panoply of signaling molecules, including Rho GTPases (Ridley 2011).

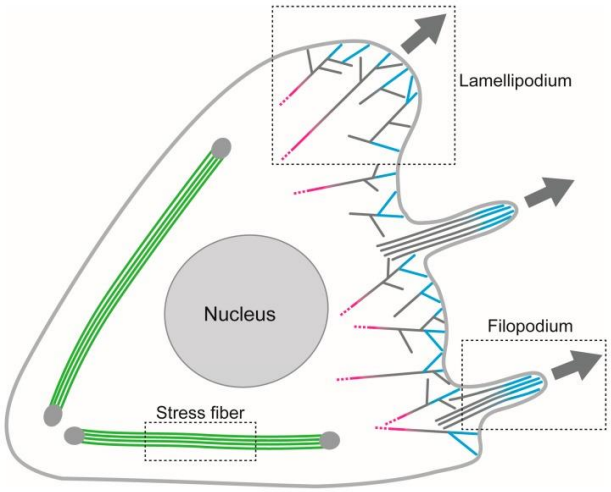

Figure 2. Actin filaments in migrating cells. Green filaments represent stress fibers, connected to FAs at their ends (grey circles). Lamellipodium and Filopodium, represented in blue, are formed at the cell membrane, in the direction of migration (Tokuraku *et al.* 2020).

1.4 Rho GTPases

The Rho family of GTPases is part of the Ras superfamily (Kalpachidou *et al.* 2019). In humans, they consist of 20 proteins, divided into 8 subfamilies according to how they are regulated, being classified as either atypical or typical/classical. Atypical subfamilies are known to be regulated by mechanisms such as expression and post-translational modifications (Haga *et al.* 2016). Typical subfamilies, on the other hand, Rho (comprising of RhoA, RhoB and RhoC), RhoF/RhoD, Rac, and Cdc42, are categorized as such considering that they act as molecular switches, cycling between an inactive GDP-bound and an active GTP-bound state (Warner *et al.* 2019). Dysregulation of Rho GTPase-dependent signaling pathways have also been linked to BC development, progression,

and to therapeutic responses (Humphries *et al.* 2020). Therefore, the correct spatiotemporal regulation of the Rho GTPases is vital for actin cytoskeleton and actin-associated adhesions dynamics control during polarized cell migration (Deakin and Turner 2008).

Rho GDP/GTP cycling is regulated by GEFs and GAPs. While the former promotes active GTP-bound formation by exchanging GDP for GTP, the latter promotes inactive GDP-bound Rho formation by stimulating the intrinsic GTPases activity of the Rho GTPase (Olayioye *et al.* 2019). Additionally, some Rho GTPases can be anchored to the plasma membrane via prenylation. By binding to the formed lipid tail, however, guanine nucleotide dissociation inhibitors (GDIs) are able to sequester Rho GTPases to the cytosol (Svensmark *et al.* 2019) – **Figure 3**.

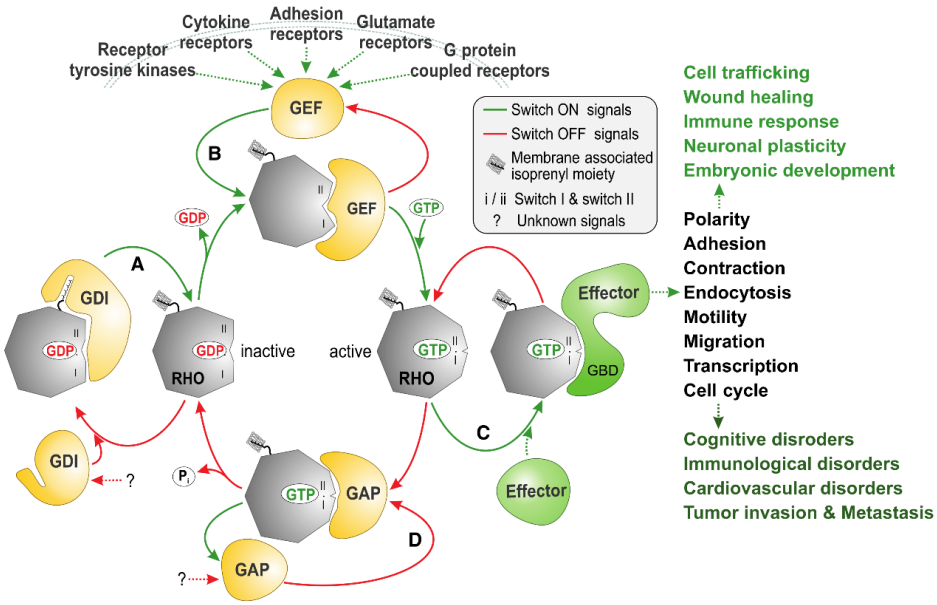

Figure 3. The Rho GTPases cycle. Typical Rho GTPases act as molecular switches, cycling between active and inactive states. **(A)** GDIs sequester Rho molecules away from the plasma membrane in resting cells, by binding to the lipid tail. **(B)** Membrane receptors activate GEF proteins, which activates Rho proteins by exchanging GDP for GTP. **(C)** Rho GTP-bound proteins interact with downstream targets through the GTPase-binding domain (GBD), controlling numerous intracellular pathways. **(D)** Rho intrinsic GTP is hydrolyzed through GTPase-activating proteins stimuli. All proteins interacting with typical Rho GTPases recognize and bind the consensus-binding sites switch I and switch II. (Mosaddeghzadeh *et al.* 2021)

RhoA is one of the best characterized Rho GTPases members (Hendrick *et al.* 2016). This Rho GTPase member, through the activation of its two targets Rho-associated, coiled-coil containing protein kinase (ROCK) 1 and ROCK2, is able to regulate stress fiber assembly and FA organization (Fagan-Solis *et al.* 2013). RhoA activation is known to cause increased formation of stress fibers and FAs, further promoting BC cell proliferation and metastasis (Seo *et al.* 2011). In fact, an increased expression of RhoA has been correlated with a poor clinical outcome (Zhang *et al.* 2016). RhoC has been identified to affect cell movement and cell adhesion and, for this reason, affecting cancer processes, most significantly by promoting metastasis in BC. As it was previously observed, RhoC depletion results in cells with abnormal wide lamellipodia with multiple branches, as a result of defective actin polymerization in the leading edge of cells. Consequently, such branches are not able to penetrate the ECM, leading to a reduction in cell migration rate (Lou *et al.* 2021).

Unlike other Rho proteins, RhoB contains a unique C-terminal region that can undergo distinct posttranslational modifications, namely farnesylation (RhoB-F) or geranylgeranylation (RhoB-GG), affecting RhoB localization and function (Ju *et al.* 2020). Due to this, RhoB is the only Rho protein that localizes not only at the plasma membrane, but also at endosomes, and has been identified at the nucleus as well. While RhoB at the plasma membrane, RhoB-F, has been associated with promoting cell growth, RhoB localizing to endosomes, RhoB-GG, has been associated with inducing cell apoptosis (Ju *et al*. 2018). Although the signaling events that underlie such differences are not yet understood, Rodriguez *et al.* observed that, unlike RhoB-GG, RhoB-F is a potent activator of the nuclear factor kappa-light-chain-enhancer of activated B cells (NF-κB), a transcription factor with a major role in proliferation and apoptosis (Rodriguez *et al*. 2007). Additionally, RhoB is also known to have a major role in regulating trafficking at the endosomes. In fact, Wallar *et al.* observed that the interplay between RhoB and the mammalian Diaphanous-related 2 formin (mDia2) GTPase effector protein was crucial for vesicle trafficking (Wallar *et al.* 2007). RhoB at the nucleus has been suggested to have a role in trafficking processes, as it was observed to functionally interact with the transcription factor DB1 (Adini *et al.* 2003). Its expression is altered in many human cancers (Karagoz *et al*. 2015). RhoB has been shown to have an enhanced expression in breast tumors and to positively correlate with malignancy (Fritz *et al.* 2002). However,

other results indicated a tumor suppressive function of RhoB in breast tumorigenesis until the tumor vasculature is established, in which RhoB then starts acting as a tumor promoter (Liu *et al.* 2000). Such paradoxical observations suggest that RhoB functions are highly context-dependent and cell-type specific (Ju *et al*. 2018). Furthermore, RhoB depletion was observed to stimulate cell migration speed and to result in cells with fewer FAs (Vega *et al.* 2012).

1.5 The RhoGEF Solo

Solo, also known as ARHGEF40 or Scambio, is a RhoGEF known to target RhoA and RhoC (Lungu *et al.* 2022). Solo comprises a C-terminal region containing a Dbl-homology (DH) domain – making this protein part of the Dbl family - and a regulatory pleckstrin homology (PH) domain, the DH-PH domain being the classical hallmark of a RhoGEF protein. (Curtis *et al.* 2004). More recently, Lungu *et al.* demonstrated that the GEF activity of Solo is able to regulate RhoB at endosomal membranes. Here, the knock down of the RhoGAP Deleted in liver cancer 3 (DLC3) was observed to result in the accumulation of RhoB at the cell periphery. However, simultaneous DLC3 and Solo knock down lead to the perinuclear re-clustering of RhoB. Such results demonstrate that to maintain the subcellular distribution of RhoB, a balanced activity of both DLC3 and Solo is necessary. Furthermore, Solo knock down in HeLa cells was observed to delay the trafficking route of Epidermal growth factor receptor (EGFR), a rapid endocytosed Receptor tyrosine kinase (RTK) upon Epidermal growth factor (EGF) ligand binding and known to be transported to the lysosomes in a RhoB-dependent manner (Lungu *et al.* 2022). Solo is also able to bind to the GTP-bound forms of Rac and Cdc42 but the function is, so far, unknown. Data from our laboratory based upon data generated by the TCGA Research Network showed that BC patients with high expression of EMT transcription factors show a higher expression of Solo (National Cancer Institute, 2021). Preliminary results from our laboratory have shown that the TNBC cell lines MDA-MB-231 and BT549 showed a higher Solo expression when compared to other BC subgroups (David Benz, unpublished data). Further results have also shown that the MDA-MB-231, BT549 and HS578T TNBC cell lines presented lower motility upon Solo depletion (Florian Meyer, unpublished data). Additionally, Solo was found to be phosphorylated

by Src at Y242, but a function has not yet been identified (Florian Meyer, unpublished data).

Solo has been identified to be involved, by association with the intermediate filaments Keratin-8/keratin-18 (K8/K18), in both tensional force-induced RhoA activation and stress fiber reinforcement. Such filaments are known to provide structural integrity to the cell against mechanical stresses (Eyckmans *et al*. 2011, Fujiwara *et al*. 2016). Additionally, Solo was observed to be necessary for K18 filaments orientation in a three-dimensional (3D) environment (Nishimura *et al.* 2018). K8/K18 filaments are able to bind to hemidesmosome proteins on the inside of the cell. Hemidesmosomes are integrin-associated proteins that assemble to form cell-specific adhesion complexes. Such complexes are known to be important for cell migration, proliferation, and other biological processes. Furthermore, hemidesmosomes formation occurs through RhoA signaling and Solo was observed to be required for their formation (Fujiwara et al. 2018).

1.6 The protooncogene Src

The non-receptor tyrosine kinase Src is one of the main effectors of FA signaling (Wu *et al.* 2016), in which increased activity was found to correlate with FAs assembly. Src is part of the Src-family kinases (SFKs), known to regulate migration, proliferation, and other cellular processes (Sawayama *et al.* 2019). SFKs can be subdivided into 9 family members in vertebrates, corresponding to modular proteins that share common domain architecture, which consists of intrinsically disordered regions (IDR) and folded domains. They incorporate a membrane-anchoring Src-homology domain 4 (SH4), the Src-homology 3 (SH3) and Src-homology 2 (SH2) regulatory domains, and Src-homology 1 (SH1) domain, the enzymatically active tyrosine kinase domain (Ortiz *et al.* 2021).

Src activity is highly regulated by intra-molecular interactions. Regarding these intra-molecular associations, some internal recognition motifs are involved. In the inactive conformation, a C-terminal tyrosine (pY527) docks with the SH2 domain. As a consequence, the SH3 domain interacts with a poly-proline motif in the SH2-kinase connector. In the active conformation, the C-terminal tyrosine is dephosphorylated (Y527) and both SH2 and SH3 domains are available for binding to substrates. Furthermore, Src is known to possess the classical kinase activation loop (A-loop), in

which Y416 tyrosine is phosphorylated (pY416) in the active form (Ingley, 2008) – **Figure 4**.

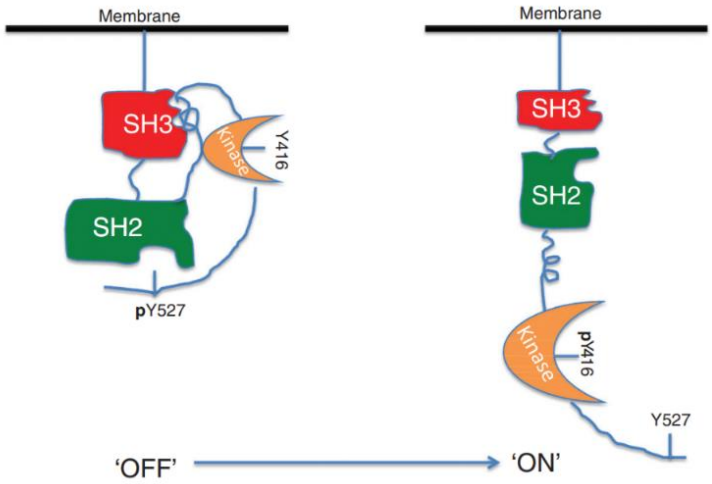

Figure 4. Src regulation. Src is formed by a SH2, SH3 and kinase domains. On the left, the inactive conformation of Src ("OFF") appears in a "closed conformation", maintained through the interaction between pY527 with the SH2 domain (green) and the SH3 domain (red) interaction with a poly-proline motif between the SH2 and kinase domain (orange). Such interactions prevent ATP and substrate binding. On the right ("ON"), the active conformation of Src ("open" conformation) is possible due to SH2/SH3 recruitment of other proteins, allowing not only for ligand binding but also autophosphorylation of the A-loop tyrosine (Y416) (adapted from Reinecke *et al*. 2014, Ortiz *et al.* 2021).

Src exhibits dual localization and distribution to the plasma membrane as well as to endosomal membrane fractions (Hikita *et al.* 2019). However, Src is mainly found at endosomal membranes, where it is inactive under non-stimulated conditions (Reinecke *et al.* 2014). Sandilands *et al*. provided evidence that Src is activated concomitantly to being translocated to the plasma membrane and that active Src localizes to vesicular structures containing RhoB. Furthermore, they showed that Src is retained at the perinuclear region in its inactive state in RhoB-null fibroblasts, indicating that RhoB is necessary for Src translocation and activation.

The way Src trafficking occurs in both normal and cancer cells is still unclear and its understanding could have crucial implications in cancer research and potential treatments. However, Src trafficking is known to be regulated by early endosomes (EE) and the actin cytoskeleton (Sandilands *et al.*2004, Reinecke *et al.* 2014). EE are the first endocytic

compartments to uptake incoming internalized cargo from the plasma membrane, in which it is later sorted to different intracellular destinations (Jovic *et al.* 2010). Additionally, *Sandilands et al.* provided evidence that Src translocation to the plasma membrane requires recycling endosomes. However, the fate of endocytic Src at the plasma membrane is not yet understood. Nonetheless, it is suggested that it might be recycled to the endocytic recycling compartment (ERC) or degraded to the lysosome pathway. In fact, Src transport was observed to be regulated by late endosomes (LE) and lysosomes as well, as active Src is hypothesized to be ubiquitinated and transported to the late endosomal-lysosomal compartment for degradation (Sandilands *et al.*2004).

1.7 Src secreted in exosomes

Exosomes, vesicle-shaped particles that export nucleic acids, proteins and lipids targeting close or distant cells, are secreted in certain physiological conditions, including by cancer cells (Nicolini *el al.* 2021). This communication mechanism can contribute to immune escape, genetic information exchange, tumor progression, invasion, and metastasis (Goh *el al.* 2020). Exosomes seem to be secreted in larger numbers in cancer cells, when compared to their non-transformed counterparts (Tickner *el al.* 2014). Piao *et al.* observed that the intercellular administration of MDA-MB-231 secreted exosomes in between BC cells promoted their migration. In cancer, activated Src is involved with enhanced exosome secretion. Furthermore, in breast, prostate, and colorectal cancers, secreted exosomes are found to be enriched in Src and its substrates, indicating that this might be a mechanism used to regulate this kinase in different cell types (Hikita *et al.* 2019, Simatou *et al*. 2020). Even though these findings may be promising, it is still not known what the crucial contents of BC secreted exosomes are. In regard to this, further research is necessary to understand the purpose of these vesicles in TNBC progression (Piao *el al.* 2018, Ramírez-Ricardo *el al.* 2020).

1.8 Breast cancer cells in three-dimensions

The vast majority of BC mechanistic studies are performed by using immortalized cell lines cultured onto two-dimensional (2D) plastic substrata (Kenny *et al.* 2007). Given that *in vivo* human cells are growing in a 3D environment, rather than a 2D one, it is extremely

relevant that cells are grown and maintained in culture similarly to the 3D conditions to better understand this pathology (Jong *et al.* 2004). Indeed, in a 3D environment cells can form aggregates that can mimic microtumors and even tissues. However, the presence of additional additives is required, for example, Matrigel, with ECM proteins in its composition, allowing a higher efficiency in the formation of tighter cell-cell and cell-ECM interactions (Badea *et al.* 2019).

MDA-MB-231, a highly aggressive, invasive, and poorly-differentiated TNBC cell line (Hong *et al.* 2010) was identified to be viable as a spheroid in 3D culture. However, apart from showing a higher resistance to antitumor compounds, levels of EMT-associated proteins were upregulated when compared to 2D adherent culture as well. Such results support the necessity of spheroid model use as promising models to understand BC mechanisms *in vivo* (Huang *et al.* 2020).

1.9 Aims of this thesis

In our laboratory, Solo was shown to have a higher expression in TNBC when compared to other BC subgroups and to be necessary for the motility of these cells. However, such mechanisms are yet to be investigated and could give valuable insights into the role of this RhoGEF protein in cell migration. Considering the major role of FAs in cell motility, the effects of Solo depletion on FA development in MDA-MB-231 and BT549 cell lines were investigated by immunofluorescence.

As a major FAs regulator, Src has not only been found to be transported in RhoB decorated vesicles but also to phosphorylate Solo. In turn, Solo was observed to be necessary for RhoB to localize at the perinuclear region of the cell. For such reasons, the subcellular localization and activity of Src in Solo depleted TNBC cells was investigated by immunofluorescence. Finally, to better understand Src localization in a 3D microenvironment, shSolo MDA-MB-231 cells were generated and cultured in a Matrigel/collagen matrix, giving further insights on how this kinase might be trafficked *in vivo*.

2. Materials

2.1 Chemicals, reagents, and solvents

Table 1. Chemicals, reagents, and solvents used.

Chemicals, reagents, and solvents	Company
4X NuPAGE™ LDS Sample Buffer	Thermo Fisher Scientific, Waltham, USA
Acrylamid (Rotiphorese Gel 30)	Carl Roth GmbH & Co., Karlsruhe, Germany
Agar-agar	Carl Roth GmbH & Co., Karlsruhe, Germany
Agarose	Carl Roth GmbH & Co., Karlsruhe, Germany
Ampicilin	Sigma Aldrich, St. Louis, USA
Complete Protease Inhibitor Cocktail (EDTA free)	Roche, Basel, Switzerland
Dimethyl sulfoxid (DMSO)	Carl Roth GmbH & Co., Karlsruhe, Germany
Dithiothreitol (DTT)	Sigma Aldrich, St. Louis, USA
Doxycycline	Sigma Aldrich, St. Louis, USA
EGTA	Carl Roth GmbH & Co., Karlsruhe, Germany
Ethanol (EtOH)	Carl Roth GmbH & Co., Karlsruhe, Germany
Ethidium bromide (EtBro)	Roche Diagnostics, Basel, Switzerland
Ethylenediaminetetraacetic acid (EDTA)	Carl Roth GmbH & Co., Karlsruhe, Germany
Glycerol	Carl Roth GmbH & Co., Karlsruhe, Germany
Gel Loading Dye Blue (6X)	New England BioLabs®, Frankfurt am Main, Germany
β-Glicerophosphate	Sigma Aldrich, St. Louis, USA
GeneRuler™ 1kb DNA ladder	Thermo Fisher Scientific, Waltham, USA
Glutamine	Thermo Fisher Scientific, Waltham, USA
Glycine	Carl Roth GmbH & Co., Karlsruhe, Germany
Goat serum	Invitrogen, Karlsruhe, Germany
HEPES	Thermo Fisher Scientific, Waltham, USA
Hydrogen chloride (HCl)	Carl Roth GmbH & Co., Karlsruhe, Germany
Isopropanol	Carl Roth GmbH & Co., Karlsruhe, Germany
Magnesium chloride ($MgCl_2$)	Carl Roth GmbH & Co., Karlsruhe, Germany

β-mercaptoethanol	Carl Roth GmbH & Co., Karlsruhe, Germany
Methanol (MeOH)	Carl Roth GmbH & Co., Karlsruhe, Germany
N,N,N,N-Tetramethyldiamin (TEMED)	Carl Roth GmbH & Co., Karlsruhe, Germany
NuPAGE™ Antioxidant	Thermo Fisher Scientific, Waltham, USA
NuPAGE™ MES SDS Running Buffer (20X)	Thermo Fisher Scientific, Waltham, USA
PageRuler™ prestained protein ladder	Thermo Fisher Scientific, Waltham, USA
Paraformaldehyde (PFA)	Carl Roth GmbH & Co., Karlsruhe, Germany
Phenylmethanesulphonyl fluoride (PMSF)	Sigma Aldrich, St. Louis, USA
Potassium chloride (KCl)	Carl Roth GmbH & Co., Karlsruhe, Germany
Potassium dihydrogen phosphate (KH_2PO_4)	Carl Roth GmbH & Co., Karlsruhe, Germany
ProLong™ Gold Antifade Reagent	Cell Signalling, Danvers, USA
Sodium azide (NaN_3)	Sigma Aldrich, St. Louis, USA
Sodium Chloride	Carl Roth GmbH & Co., Karlsruhe, Germany
Sodium deoxycholate (NaDOC)	Carl Roth GmbH & Co., Karlsruhe, Germany
Sodium dodecyl sulfate (SDS)	Carl Roth GmbH & Co., Karlsruhe, Germany
Sodium fluoride (NaF)	Carl Roth GmbH & Co., Karlsruhe, Germany
Sodium dihydrogen phosphate (NaH_2PO_4)	Carl Roth GmbH & Co., Karlsruhe, Germany
Sodium hydroxide (NaOH)	Carl Roth GmbH & Co., Karlsruhe, Germany
Sodium orthovanadat (Na_3VO_4)	Sigma Aldrich, St. Louis, USA
Sodium pyruvate	Carl Roth GmbH & Co., Karlsruhe, Germany
Thimerosal	Sigma Aldrich, St. Louis, USA
Tris-hydroxymethyl-aminomethan (Tris)	Carl Roth GmbH & Co., Karlsruhe, Germany
Triton X-100	Carl Roth GmbH & Co., Karlsruhe, Germany
Trypan Blue Solution (0.4% (w/v)	Sigma Aldrich, St. Louis, USA
Tween-20	Carl Roth GmbH & Co., Karlsruhe, Germany

2.2 Buffers and solutions

Table 2. Buffers and solutions used.

Buffer/Solution	Composition
Blocking solution (Immunofluorescence)	5% (v/v) goat serum in DPBS with $CaCl_2$ and $MgCl_2$
Blocking solution (Western blot)	0.5% (v/v) blocking solution (Carl Roth GmbH & Co. KG, Karlsruhe, Germany), 0.05% (v/v) Tween-20, 0.01% (v/v) Thrimerosal in PBS
Collagen solution	12.5% (v/v) 10X PBS, 12.5% (v/v) 0.1 M NaOH and 2.5% (v/v) 0.1M HCl in PureCol® Solution
Loading Buffer	0.5M DTT, 10% (v/v) SDS, 50% (v/v) Glycerol, 0.02% (v/v) Bromophenol blue, 1M Tris-Cl pH 6.8
Lysis buffer	150 mM Tris-Cl pH 7.5, 1% (w/v) Triton X-100, 0.1% (w/v) SDS, 150 mM NaCl, 10% glycerol, 10 mM $MgCl_2$, 0.5% sodium deoxycholate, 1 mM DTT, 0.2 mM PMSF, Complete Protease Inhibitor Cocktail, 1 Mm Na_3VO_4, 10 Mm NaF, 20 Mm β-Glicerophosphate and 1 mM EGTA in ddH_2O
Lysogeny broth (LB) agar plates	2% agar in LB medium
Lysogeny broth (LB) medium	10 g/L yeast extract and 5 g/L NaCl in ddH_2O
Paraformaldehyd (PFA)	4% (v/v) in PBS
PBS-Tween	0.05% (v/v) Tween-20 in PBS
Permeabilizing solution	0.2% (v/v) Triton X-100 in PBS
Phosphate Buffered Saline (PBS)	140 mM NaCl, 2.7 mM KCl, 8 mM Na_2HPO_4, 1.5 mM KH_2PO_4
TAE buffer	40 mM tris acetate, 1 mM EDTA in ddH_2O

2.3 Cell culture

2.3.1 Cell culture reagents

Table 3. Cell culture reagents used.

Cell culture reagents	Company
5x siRNA Buffer	Thermo Fisher Scientific, Waltham, USA
Collagen-R	Serva, Heidelberg, Germany
Dulbecco's Modified Eagle's Medium (DMEM)	Thermo Fisher Scientific, Waltham, USA
Dulbecco's Modified Eagle's Medium (DMEM) with Ca^{2+} and Mg^{2+}	Thermo Fisher Scientific, Waltham, USA
Dulbecco's Phosphate Buffered Saline (DPBS) without Ca^{2+} and Mg^{2}	Thermo Fisher Scientific, Waltham, USA

Fetal Calf Serum (FCS)	Thermo Fisher Scientific, Waltham, USA
Matrigel® Matrix	Corning, New York, USA
OptiMEM®	Invitrogen, Karlsruhe, Germany
Penicillin-streptomycin	Sigma Aldrich, St. Louis, USA
PureCol® Solution	Advanced BioMatrix, Carlsbad, USA
Puromycin	Sigma Aldrich, St. Louis, USA
RPMI 1640	Thermo Fisher Scientific, Waltham, USA
Trypsin-EDTA (10x)	Sigma Aldrich, St. Louis, USA

2.3.2 Cell culture medium

Table 4. Cell culture medium used.

Cell culture medium	Composition
2x media (3D culture)	5% FCS, 4% Matrigel® Matrix, 4 µg/mL doxycycline and 3 µg/mL puromycin in DMEM
BT549, MDA-MB-231 and HS578T medium ($DMEM^{+}$)	10% (v/v) FCS and 1% (v/v) Penicillin-streptomycin in DMEM
BT549, MDA-MB-231 and HS578T medium ($DMEM^{0.5}$)	0.5% (v/v) FCS and 1% (v/v) Penicillin-streptomycin in DMEM
Refeeding media (3D culture)	2.5% FCS, 2% Matrigel® Matrix, 2 µg/mL doxycycline and 1.5 µg/mL puromycin in DMEM
LentiX™293T medium	10% (v/v) FCS, 1% (v/v) penicillin-streptomycin, 4 mM Glutamine, 100 M HEPES, 1mM sodium pyruvate in DMEM

2.3.3 Transfection reagents

Table 5. Transfection reagents used.

Transfection reagents	Company
Lipofectamine® RNAiMAX	Invitrogen, Karlsruhe, Germany
Polybrene Infection/Transfection Reagent	Sigma Aldrich, St. Louis, USA
Polyethylenimine (PEI)	Sigma Aldrich, St. Louis, USA

2.4 Antibodies and dyes

2.4.1 Primary antibodies

Table 6. Primary antibodies used.

Primary Antibody	Species	Dilution	Identifier/Company
GAPDH	Rabbit	1:5000 (WB)	G9545/Sigma Aldrich, St. Louis, USA
Solo	Rabbit	1:2500 (WB)	20110-1-AP/Proteintech
Src	Rabbit	1:1000 (WB), 1:200 (IF)	2109/Cell signaling Technology, Danvers, USA
pSrc	Rabbit	1:1000 (WB)	6943/Cell signaling Technology, Danvers, USA
Paxillin	Mouse	1:10000 (WB), 1:300 (IF)	610052/BD Biosciences, Heidelberg, Germany
pPaxillin	Rabbit	1:1000 (WB), 1:240 (IF)	2541/Cell signaling Technology, Danvers, USA
pTyrosin (P-Tyr-99)	Mouse	1:200 (IF)	Sc-7020/Santa Cruz, Biotechnology, Dallas, USA

2.4.2 Secondary antibodies

Table 7. Secondary antibodies used.

Secondary Antibody	Species	Dilution	Identifier/Company
Alexa Fluor® 488 α-rabbit	Goat	1:500 (IF)	Invitrogen, Karlsruhe, Germany
Alexa Fluor® 647 α-mouse	Goat	1:500 (IF)	Invitrogen, Karlsruhe, Germany
HRP conjugated α-mouse	Goat	1:10000 (WB)	115-035-062/Jackson ImmunoResearch, Cambridge, USA
HRP conjugated α-rabbit	Goat	1:10000 (WB)	111-035-144/Jackson ImmunoResearch, Cambridge, USA

2.4.3 Dyes

Table 8. Dyes used.

Dye	Dilution	Identifier/Company
Alexa Fluor® 633 Phalloidin	1:2500 (IF)	Invitrogen, Karlsruhe, Germany
DAPI	1:5000 (IF)	28718-90-3/Thermo Fisher Scientific, Waltham, USA

2.5 Enzymes and Kits

2.5.1 Enzymes

Table 9. Enzymes used.

Enzyme	Company
SalI (10 U/µL)	Thermo Fisher, Rockford, USA

2.5.2 Kits

Table 10. Kits used.

Kit	Company
DC protein assay kit	Bio-Rad, Munich, Germany
HRP SuperSignal® West Substrate Pico, Picoplus, Dura Chemiluminescent Substrate	Pierve/Thermo, Rockford, USA
NucleoBond™ Xtra Midi Kit	MACHEREY-NAGEL, Düren, Germany

2.6 Oligonucleotides

2.6.1 siRNAs

Table 11. siRNAs used.

siRNA	Sequence 5'-3'	Company
ON-TARGETplus Non-targeting pool (spNT)	UGGUUUACAUGUCGACUAA	GE Healthcare, Dharmacon, USA
Silencer select Solo#2	CCUACCUAUUCACACCUGA	Ambion Inc., USA
Smart pool Solo#4	CGAGACACGCUGAACACAA	GE Healthcare, Dharmacon, USA

2.6.2 shRNAs

Table 12. shRNAs used.

shRNA	Target sequence (5'-3')	Company
shNT (pTRIPZ)	AATTCTCCGAACGTGTCACGT	GE Healthcare, Dharmacon, USA
shSolo#2	TGAGTTTGATCTCTGGTGA	GE Healthcare, Dharmacon, USA
shSolo#3	TGTGTTCAGCGTGTCTCGG	GE Healthcare, Dharmacon, USA

2.7 Plasmids

Table 13. Plasmids used.

Plasmid	Description
pCMV V-SCG	Envelope plasmid (Addgene plasmid #8454)
psPAX2	Second generation packaging plasmid (Addgene plasmid #12260)
pTRIPZ-shSolo #2	Dharmacon 305168
pTRIPZ-shSolo #3	Dharmacon 305172
pTRIPZ_nonsilencing	Non-targetting control, Dharmacon

2.8 Cell lines

Table 14. Cell lines used.

Cell line	Description	Obtained from
BT549	Triple-negative breast cancer, epithelial	CLS, Heidelberg, Germany
HS578T	Triple-negative breast cancer, epithelial	Dr. Bernhard Lüscher, RWTH Aachen, Germany
MDA-MB-231	Triple-negative breast cancer, epithelial	AG Hausser, IZI, Stuttgart, Germany
LentiX™ 293T	Human embryonic kidney cells	IBTB, Stuttgart, Germany
BT549_shNT	Stable BT549 cells expressing shNT upon doxycycline-induction	Generated in this work
BT549_shSolo#2	Stable BT549 cells expressing shSolo#2 upon doxycycline-induction	Generated in this work
BT549_shSolo#3	Stable BT549 cells expressing shSolo#3 upon doxycycline-induction	Generated in this work
HS578T_shNT	Stable HS578T cells expressing shNT upon doxycycline-induction	Generated in this work
HS578T_shSolo#2	Stable HS578T cells expressing shSolo#2 upon doxycycline-induction	Generated in this work
HS578T_shSolo#3	Stable HS578T cells expressing shSolo#3 upon doxycycline-induction	Generated in this work
MDA-MB-231_shNT	Stable MDA-MB-231 cells expressing shNT upon doxycycline-induction	Generated in this work

MDA-MB-231_shSolo#2	Stable MDA-MB-231 cells expressing shSolo#2 upon doxycycline-induction	Generated in this work
MDA-MB-231_shSolo#3	Stable MDA-MB-231 cells expressing shSolo#3 upon doxycycline-induction	Generated in this work

2.9 Equipment and consumables

2.9.1 Equipment

Table 15. Equipment used.

Equipment	Company
Amersham™ 600 (Gel and membrane imager)	GE Healthcare Life Sciences, Marlborough, USA
Avanti J-30I centrifuge (Rotor J20)	Beckman Coulter, Krefeld, Germany
Countess3 (Cell counter)	Schärfe System, Germany
ECLIPSE Ts2 Inverted microscope	Nikon Corporation, Tokyo, Japan
Electrophoresis power supply: EPS-301	GE Life Sciences, Marlborough, USA
Eppendorf Centrifuge 5415D (Rotor F45-24-11)	Eppendorf, Hamburg, Germany
Eppendorf Centrifuge 5415R (Rotor F45-24-11)	Eppendorf, Hamburg, Germany
EVOS fl. digital inverted microscope	AMG, Life technologies, Carlsbad, USA
Freezing Container Mr.Frosty™	Thermo Fisher, Rockford, USA
iBlot™	Invitrogen, Karlsruhe, Germany
IncuCyte® S3	CYTENA GmbH, Freiburg im Breisgau, Germany
LSM980 Airyscan 2 microscope	Zeiss, Jena, Germany
NanoDrop® DN-1000	Peqlab Erlangen, Germany
Pipetboy	INTEGRA biosciences GmbH, Bieberta, Germany
Pipettes (1-10µL, 2-20µL, 20-200µL, 200-1000µL)	Gilson/Eppendorf
Rotana 460 R centrifuge	Andreas Hettich GmbH & Co. KG, Tuttlingen, Germany
Stirred waterbath GD100 series	Grant Instruments, Cambridge, UK
Tecan Infinite 200 Reader	Tecan, Crailsheim, Germany

Thermoshaker MKR 13	HLC BioTech, Bovenden, ermany
Varocell 2460, CO_2 incubator	Varolab, Gieβen, Germany
Vortex-Genie 2	Scientific Industries, Bohemia, New York, USA
Work bench Laminar flow class 2 work	Varolab, Gieβen, Germany

2.9.2 Consumables

Table 16. Consumables used.

Consumable	**Company**
Bacteria petri dishes	Greiner Bio-One GmbH, Frickenhausen, Germany
Cell culture flasks, plates, and dishes	Greiner Bio-One GmbH, Frickenhausen, Germany
Cell scrapers	Corning, Kaiserslautern, Germany
Cellstar™ 96 well plate flat bottom	Greiner Bio-One GmbH, Frickenhausen, Germany
Cellstar™ tubes (15mL and 50mL)	Greiner Bio-One GmbH, Frickenhausen, Germany
Coverslips (18 mm x 18 mm) and slides (microscopy)	Car Roth GmbH & Co., Karlsruhe, Germany
Cryo Vials	Greiner Bio-One GmbH, Frickenhausen, Germany
Falcon® CultureSlides (8 Chamber Polystyrene Vessel Tissue Culture Treated Glass Slide)	Corning Inc., New York, USA
iBlot®Gel Transfer Stacks Nitrocellulose, Regular	Invitrogen, Karlsruhe, Germany
NuPAGE™ 4-12% Bis-Tris Midi Gel	Thermo Fisher Scientific, Waltham, USA
Parafilm® M	Bemis Corporate, Neenah, USA
Pipette tips (1-10µL, 2-200µL, 200-1000µL)	Greiner Bio-One GmbH, Frickenhausen, Germany
Reaction tubes (1.5mL/2mL, standard and safe-lock)	Eppendorf, Hamburg, Germany
Serological pipettes (2mL/5mL/20mL/25mL)	Corning, Kaiserslautern, Germany
Syringe filter (0.45µm)	Sarstedt AG & Co. KG, Nümbrecht, Germany
Syringe Omniflix (5mL)	Carl Roth Gmbh & Co., Karlsruhe, Germany

2.10 Software

Table 17. Software used.

Software	Company
GraphPad Prism 8	Graphpad Holdings LCC, San Diego, USA
ImageJ (Fiji)	GitHub, San Francisco, USA
IncuCyte® S3 2019A	Essen Bioscience, Inc., Michigan, USA
Microsoft Office	Microsoft, Redmond, USA
Zen 3.1 (blue edition)	Zeiss, Jena, Germany

3. Methods

3.1 Cell culture

All cell lines were cultivated at 37 °C and 5% CO_2. BT549, HS578T and MDA-MB-231 cells were cultivated in $DMEM^+$ media (DMEM supplemented with 10% FCS (v/v) and 1% (v/v) Penicillin-streptomycin). Stable BT549, HS578T and MDA-MB-231 cells were cultivated in $DMEM^+$ media supplemented with 1.5µg/mL puromycin. To induce the expression of the construct, 2µg/mL of doxycycline were added to the media for a total of 72 hours. LentiX 293T cells were cultivated in $DMEM^{++}$ media (DMEM supplemented with 10% (v/v) FCS, 1% (v/v) penicillin-streptomycin, 4 mM Glutamine, 10 mM HEPES and 1mM sodium pyruvate).

Cells were passaged every 2-3 days, keeping confluency below 90%. For the splitting, cells were washed with PBS (without Ca^{2+} and Mg^{2+}) and incubated in 1x Trypsin-EDTA solution for 5 minutes at 37 °C. Afterwards, cells were resuspended in the respective media, centrifugated at 1500 rpm for 3 minutes and, once again, resuspended in the respective media. For cells maintenance, cells were diluted in a 1:3 or 1:4 ratio, considering cells confluency. For specific experimental use, cells were counted by mixing cells suspension with Trypan Blue solution in a 1:1 ratio and using the Countess3.

For long term storage of the stable BT549, HS578T and MDA-MB-231 cell lines, a total of 1.0×10^6 cells/mL were resuspended in DMSO supplemented with 10% (v/v) FCS. The cells suspension was added to cryovials, which were frozen at -80 °C in Mr.Frosty™ freezing containers. After a period of 24 hours the cryovials were transferred into liquid nitrogen. For the thawing of frozen cells, cryovials were transferred to a 37 °C water bath for 2 minutes, resuspended in pre-warmed $DMEM^+$ media and centrifugated at 1500 rpm for 3 minutes. Afterwards, the pellet was resuspended in pre-warmed $DMEM^+$ media and transferred to a cell culture flask.

3.2 Transformation of *Escherichia coli,* plasmid amplification and isolation

The generated plasmids (previously generated in the laboratory) were transformed into chemically competent *Escherichia coli* strain Stbl3 by the heat shock method. For this, bacteria were thawed on ice, DNA was added (15 ng/100 µL of cells) and incubated for 10 minutes on ice. After a heat shock of 42 °C for 45 seconds bacteria were recovered on ice for 5 minutes. Afterwards, the culture was inoculated in LB medium and bacteria recovered after 1 hour at 37 °C with horizontal shaking. Bacteria were plated on LB-Agar plates supplemented with 1 µL/mL ampicillin. After 10 hours of incubation at 37 °C single colonies were picked.

The picked colonies were incubated in LB medium supplemented with 1 µL/mL ampicillin overnight at 37 °C and subsequently harvested. For the plasmids isolation the NucleoBond™Xtra Midi Kit was used and DNA concentrations measured with Nanodrop.

To verify the insertion of the ligated DNA fragments, the isolated plasmid DNA was subjected to restriction digestion and its products analyzed by agarose gel electrophoresis at 70 V for 1 hour.

3.3 Generation of stable cell lines

Stable cell lines expressing different shRNA constructs were generated by Lentiviral transduction of BT549, HS578T and MDA-MB-231 cells. For viral production, 2.5×10^6 LentiX 293T cells were cultivated in 15 cm dishes with a total volume of 30 mL of $DMEM^{++}$ media. After 72 hours, to achieve a confluency of 70-90 %, media was removed and 23 mL of pre-warmed fresh media was added. For the PEI transfection, the transfection mix was prepared in 15 mL Falcon Tubes, according to the reagent volumes listed in **Table 18**. The plasmids of interest are listed in **Table 13**. After 15 minutes of incubation at room temperature (RT) the transfection mix was added dropwise to the LentiX 293T cells.

Table 18. Transfection mix used for PEI transfection of LentiX 293T cells.

Reagent	Volume
OptiMEM®	2.5 mL
pCMV V-SVG	4.5 µg
psPAX2	9 µg
Plasmid of interest (DNA)	18 µg
PEI	94.5 µg

The next day, LentiX 293T cells were washed once with pre-warmed $DMEM^+$ media and 13 mL of pre-warmed fresh $DMEM^+$ media was added to the dishes. Parallelly, for the infection, a total of 3.0×10^5 cells, for each BT549, HS578T and MDA-MB-231 cell line, were cultivated in 9.6 cm^2 wells with 2.5 mL of $DMEM^+$ media.

24 hours later, the LentiX 293T cells media was collected and 13 mL of pre-warmed fresh $DMEM^+$ media was added to the dishes. The collected media enriched with the virus was centrifugated at 1500 rpm for 3 minutes and the supernatant was drawn up with a sterile syringe and filtered with a sterile 0.45 µm filter. The media of the previously cultivated TNBC cells was removed and 3 mL of the filtered supernatant, supplemented with 8 µg/mL of polybrene, was added to the cells. The remaining supernatant was stored at -80 °C. On the same day, the LentiX 293T cells media was once again collected and filtered the same way as previously and added again to the TNBC cells.

On the next day, the target cells media was removed, cells were washed once with PBS and fresh 3 mL pre-warm media was added to the wells. One day after the infection, cells were selected with 1.5 µg/mL puromycin. Once 80% confluency was achieved, cells were replated.

3.4 Puromycin titration

To determine the minimum amount of antibiotic required to kill non-transfected cells, 2.0×10^4 cells/cm^2 of BT549, HS578T and MDA-MB-231 cell lines were cultivated overnight at 37 °C in $DMEM^+$ in 9.6 cm^2 dishes. Afterwards, the media was replaced with fresh pre-warmed $DMEM^+$ supplemented with 3 different puromycin concentrations (1.5 µg/mL, 5 µg/mL and 8 µg/mL), as well as untreated control without antibiotic for all 3 cell lines. 4 days later cells viability was assessed for minimal antibiotic concentration that efficiently killed non-transfected cells.

3.5 siRNA cell transfection

For each reverse-transfection, 150 µL OptiMEM®, 4.2 µL Lipofectamine® RNAiMax and an end-concentration of 5 nM of the siRNA of interest were added to a 9.6 cm^2 after pre-incubation of the master mix at RT for 10 minutes. 3.0×10^5 cells/mL were added and incubated at 37 °C with a total volume of 2.5 mL of $DMEM^+$ for 72 hours. ON-TARGETplus Non-targeting Pool was used as a control. All siRNA's used are listed in **Table 11**.

3.6 Cell lysis and protein concentration determination

72 hours after siRNA transfection of cells in $DMEM^+$ or doxycycline induction of stable cells in $DMEM^+$ supplemented with 1.5 µL/mL puromycin in 9.6 cm^2 dishes (2.0×10^5 cells/mL), cells were washed once with PBS (without Ca^{2+} and Mg^{2+}) and incubated in 1x Trypsin-EDTA solution for 5 minutes at 37 °C. Afterwards, cells were centrifugated at 1500 rpm for 3 minutes and resuspended in $DMEM^{0.5}$. Cells were then plated in new 9.6 cm^2 dishes previously coated with 1:80 Collagen R, either for 2 hours at 37 °C or overnight at 4 °C, with 2,5 mL of $DMEM^{0.5}$ for 4 hours at 37 °C.

For the lysis, the 9.6 cm^2-dish plates were placed on ice and washed with 2 mL of cold PBS and lysed with 300 µL lysis buffer. Cells were collected with a cell scraper, incubated for 15 minutes on ice and centrifugated at 15000 rpm at 4 °C for 10 minutes. The supernatant was transferred to new reaction tubes.

Protein concentration was measured using the DC™ Protein Assay. With the Tecan Spark® microplate reader the absorbance was determined at 750 nm. Samples were diluted with lysis buffer to the lowest measured concentration.

For the hot lysis protocol, a loading buffer was pre-warmed at 95 °C, added directly to the 9.6 cm^2 dishes and cells collected with a cell scraper. Cells were then centrifugated at 15000 rpm for 15 minutes at RT. For this protocol protein concentration was not measured.

3.7 SDS polyacrylamide gel electrophoresis (SDS-PAGE)

Samples for SDS-PAGE were mixed with 4X NuPAGE® LDS Sample Buffer, cooked at 70 °C for 10 minutes and DTT with an end-concentration of 50 mM was added. Samples were either directly used for SDS-PAGE or stored at -20 °C.

For the SDS-PAGE running, 20 µL of cell lysates were loaded onto a NuPAGE® 4-12% Bis-Tris gel, as well as 2 µL of the PageRuler™ prestained protein ladder marker. To the SDS-PAGE chamber, 1X NuPAGE® MES SDS running buffer was added with 435 µL of NuPAGE® Antioxidant. Gels were run at 200 V for 55 minutes. Afterwards, Western blotting was performed.

3.8 Western Blotting

After electrophoresis, the now separated proteins were transferred onto a nitrocellulose membrane for 8 minutes and 40 seconds using the iBlot device. To block unspecific antibody binding, membranes were incubated in western blocking solution for 1 hour on a shaker at RT. Afterwards, membranes were cut and incubated overnight with primary antibodies (**Table 6**), diluted in western blocking solution with 1% sodium azide on a roller at 4 °C.

Membranes were washed 3 times, 5 minutes each, with 1X PBS-Tween. After incubation with the respective HRP-conjugated secondary antibody (1:10000) in western blocking solution on a shaker at RT for 1 hour, membranes were washed the same way as previously described. SuperSignal™ West Dura Extended Duration Substrate or SuperSignal™ West Pico Plus Chemiluminescent Substrate was added to the membrane and incubated for 5 minutes in dark conditions at RT. Signals were detected with the Amersham 600. Signals were normalized to GAPDH and quantified using the software ImageJ.

3.9 3D cell culture

One day before the seeding, an appropriate amount of Matrigel® Matrix was left on ice at 4 °C. Sterile tips, reaction tubes and 8-well cell culture slides isolated with Parafilm® were stored at -20 °C.

For each 8-well cell culture slide chamber a total of 80 µL of 1:1 Matrigel® Matrix and Collagen Solution was added, followed by 30 minutes incubation at 37 °C for solidification. All steps were performed on ice with cold tips and reaction tubes.

Parallelly, 72 hours after doxycycline induction of stable cells in 9.6 cm^2 dishes (2.0×10^5 cells/mL) in $DMEM^+$ supplemented with 1.5 µL/mL puromycin, cells were washed once with PBS (without Ca^{2+} and Mg^{2+}) and incubated in 1x Trypsin-EDTA solution for 5 minutes at 37 °C. Afterwards, cells were centrifugated at 1500 rpm for 3 minutes and resuspended in DMEM for a final concentration of 1.0×10^4 cells/mL.

Once solidification was achieved, for each chamber, 100 µL of 2x media was added on top, as well as 100 µL from the prepared cell suspension. Cells were then incubated at 37 °C for 7 days, with a media exchange of 200 µL refeeding media every 2-3 days. Spheroid formation and cell viability was observed with EVOS fl. digital inverted microscope every exchaging media day.

3.10 2D immunofluorescence

Microscopy coverslips were coated with 1:80 Collagen R in PBS for 2 hours in the incubator at 37 °C or overnight at 4 °C. After incubation, coverslips were washed twice with PBS. Pre-warmed $DMEM^{0.5}$ was added on top.

72 hours after siRNA transfection of cells in 9.6 cm^2 dishes (2.0×10^5 cells/mL) in $DMEM^+$ or doxycycline induction of stable cells in $DMEM^+$ supplemented with 1.5 µL/mL puromycin, cells were washed once with PBS (without Ca^{2+} and Mg^{2+}) and incubated in 1x Trypsin-EDTA solution for 5 minutes at 37 °C. Afterwards, cells were centrifugated at 1500 rpm for 3 minutes and resuspended in $DMEM^{0.5}$. 3.0×10^4 cells/mL were replated on the Collagen R coated coverslips and incubated for 4 hours at 37 °C.

For fixation and permeabilization, cells were washed once with PBS-$Ca^{2+}Mg^{2+}$ at RT and incubated with 4% PFA with 0.1% Triton at RT. After 10 minutes, cells were washed 3 times, 5 minutes each, with PBS-$Ca^{2+}Mg^{2+}$. Cells were then blocked with blocking solution at RT for 1 hour.

Primary antibodies were diluted in blocking solution and coverslips were incubated in 60 µL primary antibody dilution at 4 °C overnight. Coverslips were then washed 3 times, 5 minutes each, with PBS-$Ca^{2+}Mg^{2+}$ and incubated with Alexa Fluor™ coupled secondary antibodies and/or Alexa Fluor™-633 coupled Phalloidin and DAPI for 2 hours at RT and in dark conditions. Coverslips were washed 3 times, 5 minutes each, with PBS-$Ca^{2+}Mg^{2+}$ and mounted with ProLong™ Gold Antifade Reagent at RT overnight.

Images were aquired using the LSM980 Airyscan 2 microscope (63x oil-immersion objective) and analysed with ZEN 3.1. Image stacks from samples are shown as maximum intensity projections. Excitation wavelenghts and detection window used are listed in **Table 19**.

Table 19. Excitation wavelenghts and detection window used.

	Excitation wavelenght (nm)	**Detection window (nm)**
Alexa Fluor®-546 coupled Phalloidin	561	573-621
Alexa Fluor®-633 coupled Phalloidin/Alexa Fluor® 647 α-mouse	633	650-717
DAPI	405	425-488
Alexa Fluor® 488 α-rabbit	488	496-550

3.11 3D immunofluorescence

After the completion of the 7 days for the stable cells growth in 3D conditions, each well was washed once with pre-warmed PBS-$Ca^{2+}Mg^{2+}$. Cells were fixed with 2% PFA in PBS-$Ca^{2+}Mg^{2+}$ for 15 minutes in the incubator at 37 °C. Cells were then washed with PBS-$Ca^{2+}Mg^{2+}$ 3 times, 5 minutes each, and quenched with 150 mM Glycine in PBS-$Ca^{2+}Mg^{2+}$ for 15 minutes at RT. Afterwards, cells were washed 3 times, 5 minutes each, with PBS-$Ca^{2+}Mg^{2+}$ and permeabilization was performed with 0.5% Triton in PBS-$Ca^{2+}Mg^{2+}$ for 10 minutes at RT. Cells were again washed 3 times, 5 minutes each, with PBS-$Ca^{2+}Mg^{2+}$ and blocking was performed with blocking solution for 45 minutes at RT.

Primary antibodies were diluted in blocking solution and 8-well cell culture slides were incubated in 150 µL primary antibody dilution at 4 °C overnight.

Each chamber was washed 5 times, 5 minutes each, with PBS-$Ca^{2+}Mg^{2+}$ and incubated with Alexa Fluor™ coupled secondary antibodies and DAPI for 2 hours at RT and in dark

conditions. Each chamber was washed 2 times, 5 minutes each, with PBS-$Ca^{2+}Mg^{2+}$. The 8-well cell culture slides plastic protection was carefully removed and the Matrigel/Collagen bed was mounted with ProLong™ Gold Antifade Reagent at RT overnight.

Images were aquired using the LSM980 Airyscan 2 microscope (63x oil-immersion objective) and analysed with ZEN 3.1 software. Image stacks from samples are shown as maximum intensity projections. Excitation wavelenghts and detection window used are listed in **Table 19**.

3.12 Statistical analysis

For statistical analysis of the results, GraphPad Prism 8 was used. The comparison between all values was performed by a one-way analysis of variance (ANOVA) followed by Brown-Forsythe and Welch tests (not assuming equal standard deviations). "N" refers to the total number of samples for each experiment while "n" refers to the number of independent experiments performed. The calculated p-values are indicated in the figures to mark significance as follows: $p > 0.05$ (ns), $p \leq 0.05$ (*), $p \leq 0.01$ (**), $p \leq 0.001$ (***) and $p \leq 0.0001$ (****).

4. Results

Triple-negative breast cancer (TNBC) is the most aggressive group of breast cancer (BC), having the highest rate of metastatic occurrence (Sun *et al.* 2020). In metastasis cell migration is necessary (Khaled *et al.* 2019). The protein Solo is known to regulate Rho GTPases (Mosaddeghzadeh *et al.* 2021), which are important for cell migration (Humphries *et al.* 2020).

MDA-MB-231, BT549 and HS578T cell lines have been shown to present lower motility upon Solo depletion (Florian Meyer, unpublished data). These results indicate that Solo might have an important role in TNBC aggressiveness and in cell migration. However, the molecular mechanisms and the pathological roles of Solo are yet to be understood (Fujiwara *et al.* 2018).

4.1 Solo depleted MDA-MB-231 and BT549 cells showed increased Paxillin intensity at FAs

Solo has an important role in TNBC cells motility (Florian Meyer, unpublished data), a biological process in which focal adhesions (FAs) are crucial, serving as anchorage (Wang *et al.* 2018). These structures are typically coupled with the actin cytoskeleton (Deakin and Turner 2008). The cytoskeleton reorganization, in turn, is regulated by Rho GTPases (Isozaki *et al.* 2020). Given that Solo is a RhoGEF (Lungu *et al.* 2022), it was hypothesized that FAs might be altered by the depletion of Solo. To test whether Solo knock down affects FAs size, the FA resident scaffolding protein Paxillin was used as a FA marker and stained in an immunofluorescence. Thus, MDA-MB-231 and BT549 cells were seeded and transfected with one of two independent previously validated siRNAs targeting Solo or a control siRNA. 72 hours later, cells were seeded onto Collagen R coated coverslips for 4 hours, cells were fixed, permeabilized and stained for Paxillin. Paxillin was then quantified at the FAs, each value representing the mean fluorescence intensity (MFI) of one isolated FA.

Paxillin MFI at the FAs was increased upon Solo knock down in MDA-MB-231 cells - **Figure 5A**. siNT transfected cells showed a MFI of 6.491 arbitrary units (a.u.), while the MFI of siSolo ss#2 and siSolo sp#4 transfected cells showed an increase to 9.397 a.u. and

8.882 a.u., respectively - **Figure 5B**. Similarly, these results were also observed for the BT549 cells – **Figure 5A**, in which siNT transfected cells showed a MFI of 6.849 a.u., while the MFI of siSolo ss#2 and siSolo sp#4 transfected cells showed an increase to 9.619 a.u. and 8.959 a.u., respectively - **Figure 5B**. In conclusion, FAs appear to be larger upon Solo knock down for both TNBC cell lines, as a result of increased Paxillin MFI at the FAs. In HeLa cells, Solo was observed to be involved in the regulation of RhoB activity on endosomes, a GTPase with a central role in endocytic trafficking (Lungu *et al.* 2022). For this reason, the trafficking of FA complex proteins which are trafficked in a RhoB dependent manner might be altered upon Solo knock down. Thereby, it would be relevant to investigate this next.

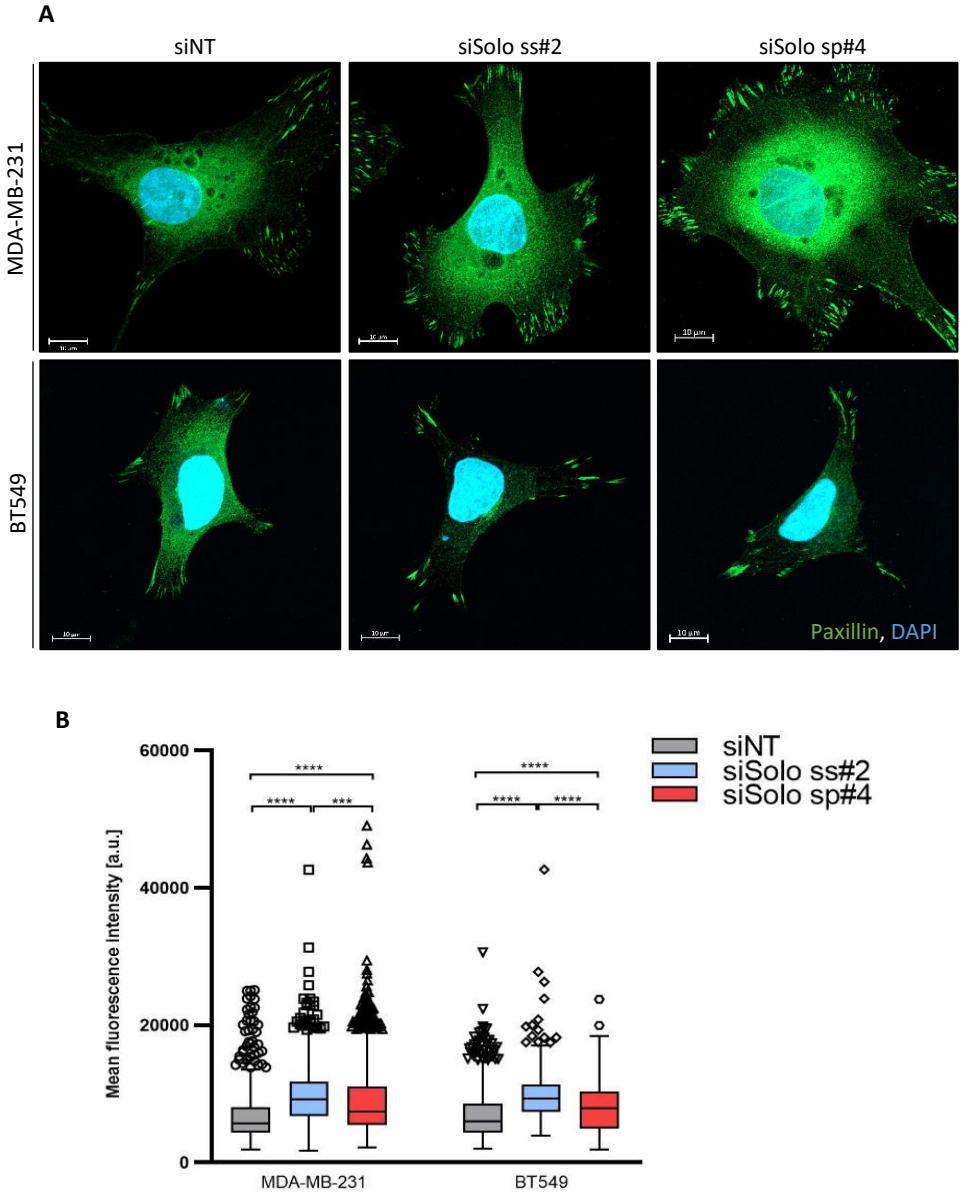

Figure 5. Paxillin at focal adhesions is increased upon transient Solo knock down. MDA-MB-231 and BT549 cells were transfected with siSolo (ss#2 or sp#4) or a non-targeting control (siNT) and cultivated for 72 hours. 8.300 cells·cm^{-2} were seeded onto Collagen R coated coverslips, fixed 4 hours later and stained for Paxillin (green) and DNA counterstained with DAPI (blue). **(A)** The images are maximum intensity projections of several confocal sections. Scale bars: 10µm. **(B)** The mean fluorescence intensity of the Paxillin signal was assessed and plotted in a tukey-boxplot. Brown-Forsythe and Welch ANOVA comparison tests for each cell line were performed. (n=3; N=24 (siNT), 25 (siSolo ss#2, siSolo sp#4) for MDA-MB-231 and n=3, N=26 (siNT, siSolo sp#4); n=2, N=18 (siSolo ss#2) for BT549)

4.2 Solo knock down in MDA-MB-231 and BT549 cells lead to Src accumulation at the perinuclear region

One of the main effectors of FA signaling is Src (Wu et al. 2016). In fact, Src loss or inhibition is associated with more stable FAs (Koudelková et al. 2021). Additionally, this kinase is known to be translocated in between the plasma membrane and endosomal membrane fractions (Hikita *et al.* 2019) in a RhoB dependent manner (Reinecke *et al.* 2014). Thus, it was hypothesized that the depletion of Solo could regulate Src trafficking via RhoB and, as a consequence, localization. Ergo, the distribution of Src was assessed in control and Solo depleted cells by immunofluorescence. Thereby, MDA-MB-231 and BT549 cells were seeded and transfected with one of two independent previously validated siRNAs for Solo knock down or a control siRNA. 72 hours later, cells were seeded onto Collagen R coated coverslips for 4 hours and cells were later fixed, permeabilized and stained for Src.

MDA-MB-231 cells with depleted Solo exhibited strong Src accumulations at the perinuclear region of the cell, for both siRNAs. In contrast, siNT cells exhibited a more homogeneous Src distribution across the cell, with a slight increase of Src at the perinuclear region. However, BT549 cells seemed to have a more homogeneous distribution of Src for both Solo targeting as well as control siRNAs – **Figure 6**. These results indicate that, in MDA-MB-231 cells, Solo may affect Src localization, since depletion of the former leads to the accumulation of the latter at the perinuclear region. Since the localization of Src in between the perinuclear region and FAs was altered upon Solo depletion, Src activity and Paxillin phosphorylation, as a downstream target, would be worth investigating next.

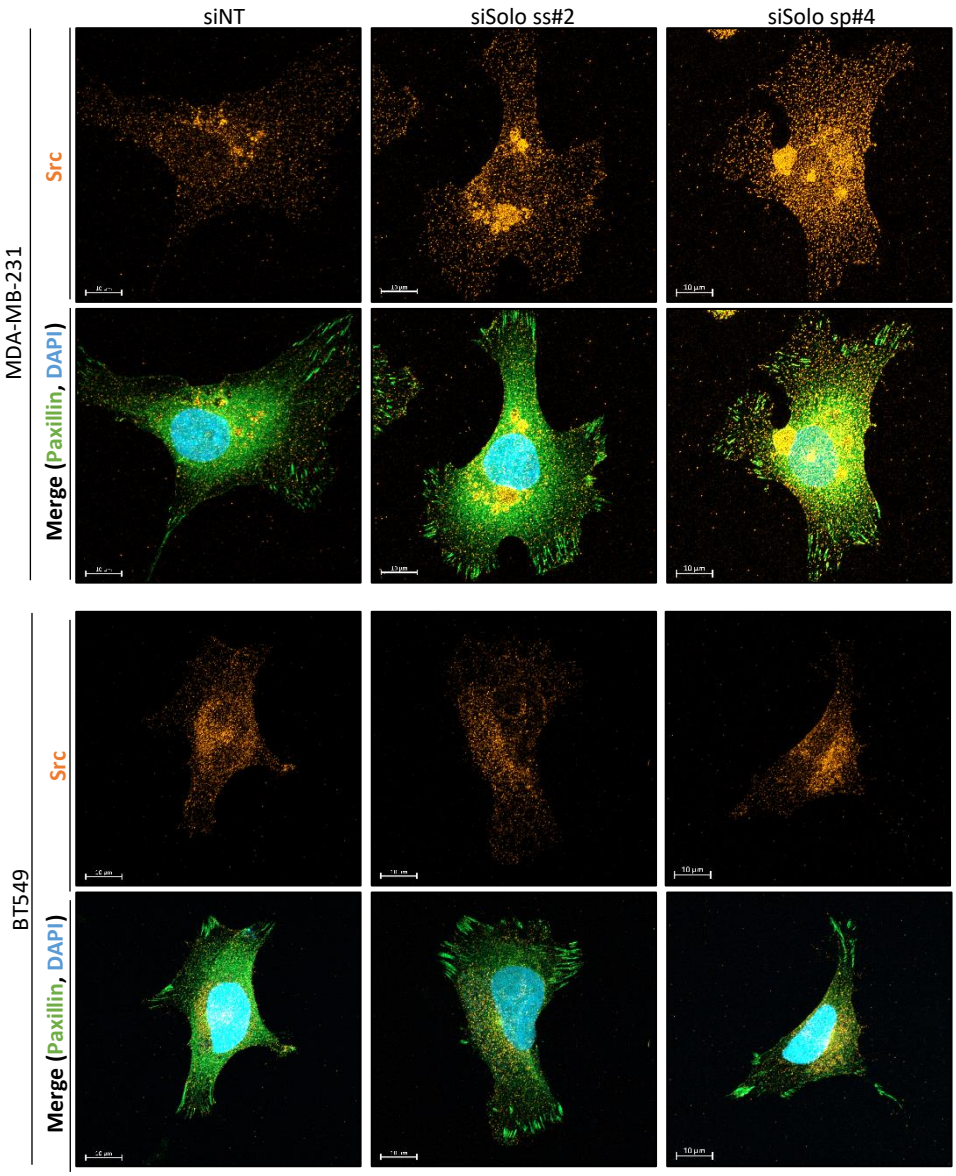

Figure 6. Src accumulates at the perinuclear region upon knock down of Solo in MDA-MB-231 cells. MDA-MB-231 and BT549 cells were transiently transfected with siSolo (ss#2 or sp#4) or a non-targeting control (siNT) for 72 hours. Afterwards 8.300 cells·cm^{-2} were seeded onto Collagen R coated coverslips, fixed 4 hours later and stained for Src (orange), Paxillin (green) and DNA counterstained with DAPI (blue). The images are maximum intensity projections of several confocal sections. Scale bars: 10µm. (n=3)

4.3 Solo depleted MDA-MB-231 and BT549 cells showed an altered relative amount of phosphorylated Src and Paxillin

To further understand the effects that Solo knock down might have on Src activity, MDA-MB-231 and BT549 cells were seeded and transfected with one of two independent previously validated siRNAs for Solo knock down or a control siRNA. Cells were lysed

72 hours later and active Src (pSrc) and phosphorylated Paxillin (pPaxillin) levels were analyzed by western blot.

Src activity increased upon Solo depletion, with a 1.8-fold increase for both siSolo transfected MDA-MB-231 cells. Src activity decreased upon Solo depletion with a two- and nine-fold decrease for the siSolo ss#2 and siSolo sp#4 transfected BT549 cells, respectively. Paxillin phosphorylation increased upon Solo depletion. This increase was larger for the siSolo sp#4 treated MDA-MB-231 cells, with a 2.4-fold increase, while for siSolo ss#2 treated cells a 1.3-fold increase was registered. This increase was also larger for the siSolo sp#4 treated BT549 cells, with a 1.9-fold increase, while for siSolo ss#2 treated cells a 1.3-fold increase was registered. Considering that Solo levels were strongly decreased, the siRNAs mediated knock down worked as expected - **Figure 7**. Overall, these results indicate an increase in relative phosphorylated Paxillin upon Solo knock down for both TNBC cell lines and that the effects on Src activity are not conserved in MDA-MB-231 and BT549, since it increases in the former but decreases in the latter.

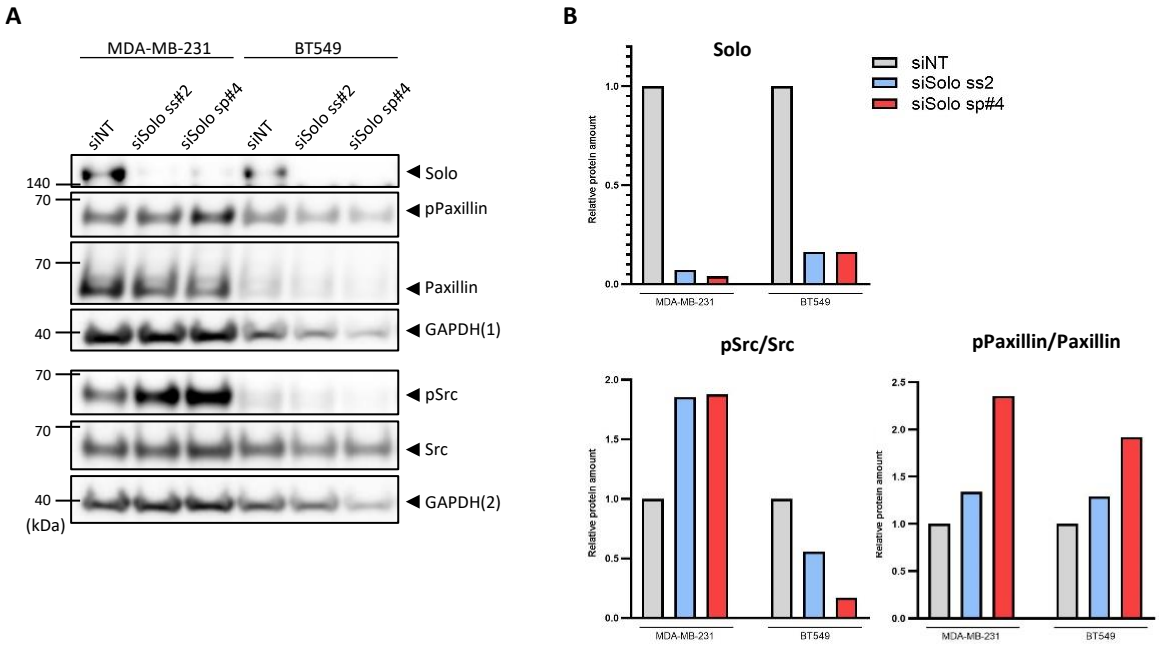

Figure 7. Focal adhesion signaling is altered by transient knock down of Solo in MDA-MB-231 and BT549 cells. **(A)** MDA-MB-231 and BT549 cells were transiently transfected with siSolo (ss#2 or sp#4) or a non-targeting control (siNT) and cultivated for 72 hours. 101.000 cells·cm^{-2} were seeded onto a Collagen R coated surface and lysed using a hot lysis protocol 4 hours later. Solo, pY118-Paxilllin (pPaxillin) and Paxillin were normalized to GAPDH (1). pY416-Src (pSrc) and Src were normalized to GAPDH (2). **(B)** Normalized signal to siNT from (A) shown as bars. (n=1)

4.4 Stable shSolo cells were successfully generated

To enable long-term experiments such as three-dimensional (3D) culture, stable cell lines expressing either the control shNT or the Solo-targeting shSolo#2 or shSolo#3 were generated by Lentiviral transduction of BT549, MDA-MB-231 and HS578T cells. The shRNAs are expressed in a doxycycline-inducible manner. Due to the co-expression of TurboRFP, the induction can be verified microscopically. Considering time limitations, further experiments were focused on the stable shSolo MDA-MB-231 cell line.

Firstly, to validate the expression of the shRNAs in the generated stable MDA-MB-231 cell lines, cells were treated with doxycycline for 72 hours to induce their expression. Doxycycline induction was validated through the expression of TurboRFP by fluorescence microscopy. While strong signals were detected for the doxycycline induced cells, untreated ones showed no signal, indicating there is no leaky expression – **Figure 8A**. To confirm Solo knock down, cells were lysed in parallel and Solo levels were analyzed by western blot. As expected, Solo protein levels were reduced for both shSolo#2 and shSolo#3 cell lines by 95% and 97%, respectively – **Figure 8B**. To characterize cells morphology, immunofluorescence was performed. For this reason, 72 hours doxycycline-induced cells were seeded onto Collagen R coverslips and, 24 hours later, fixed, permeabilized and F-actin stained with Alexa Fluor-488 labelled Phalloidin. For all cell lines two phenotypes were observed: (1) cells with an irregular shape with the absence of a strong F-actin signal at the membrane and (2) cells with a circular shape with a strong aforementioned F-actin signal. Irregular shaped shNT cells showed stronger F-actin signal in comparison to shSolo ones. However, no further differences were observed in between shNT, shSolo#2 and shSolo#3 cell lines – **Figure 8C**. Overall, the shRNAs led to an efficient decrease in Solo levels and thus further studies were conducted using these cells.

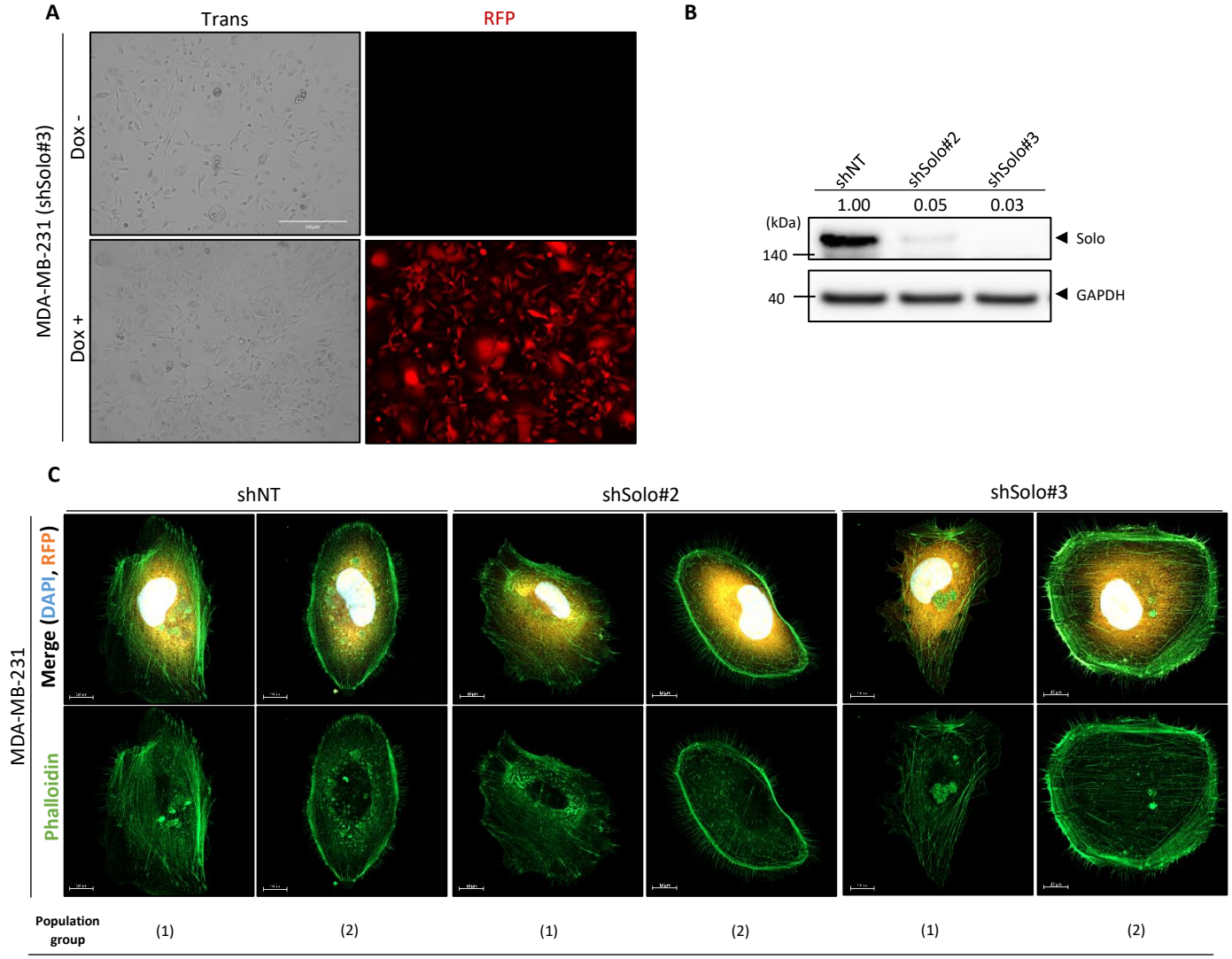

Figure 8. Characterization of stable MDA-MB-231 cells with doxycycline-inducible shSolo expression. (A) Fluorescence microscopy images of RFP expression in stable shSolo#3 MDA-MB-231 cells, cultured simultaneously with or without doxycycline for 72 hours. Scale bars: 300µm. **(B-C)** 42.000 cells·cm^{-2} cells of the stable MDA-MB-231 cell lines were cultured, and expression of Solo was induced with doxycycline. After 72 hours cells were lysed and **(B)** relative Solo expression levels quantified. GAPDH was used as a loading control **(C)**, and 8.300 cells·cm^{-2} seeded onto Collagen R coated coverslips, fixed 4 hours later, DNA counterstained with DAPI (blue) and actin stained with Alexa Fluor-488 labelled Phalloidin (green). (1) and (2) represent distinct observed morphological populations. Scale bars: 10µm. (n=1; N=9 (shNT, shSolo#2, shSolo#3))

4.5 shSolo MDA-MB-231 cells showed decreased Src activity and increased levels of phosphorylated Paxillin

To validate the previous observed effects on Paxillin and Src activity upon transient Solo depletion, the stable MDA-MB-231 cells were lysed after 72 hours of doxycycline induction and protein levels were analyzed by western blot.

Src activity was decreased for both shSolo#2 and shSolo#3, with a 1.25- and a two-fold decrease, respectively. On the other hand, the phosphorylation of Paxillin at the Y118

residue increased for both shSolo#2 and shSolo#3 cell lines, with a 1.4- and 1.3-fold increase, respectively – **Figure 9**. In conclusion, these results indicate a reduction in Src activity and an increase in Paxillin phosphorylation at the residue Y118 for the shSolo MDA-MB-231 cells. Since these results were contradicting to the previously observed ones, the subcellular localization of Paxillin was investigated in an immunofluorescence.

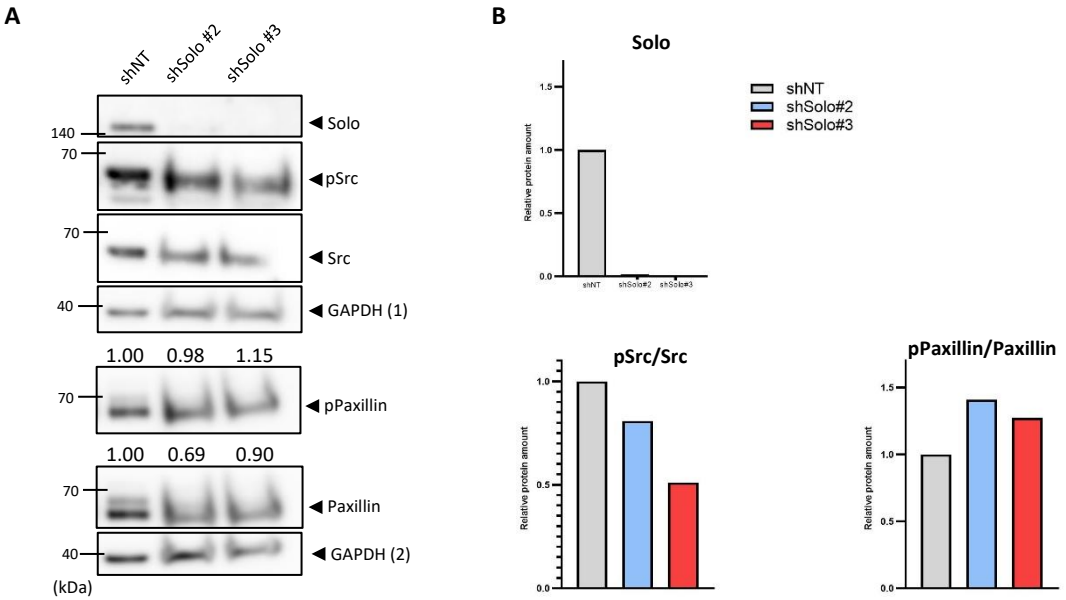

Figure 9. Relative amount of phosphorylated Src decreases and phosphorylated Paxillin increases in stable shSolo MDA-MB-231 cells. Relative amount of Solo, pPaxillin, Paxillin, pSrc and Src of stable MDA-MB-231 cells. **(A, B)** Cells were simultaneously seeded with or without doxycycline for 72 hours. 36.000 cells·cm^{-2} were seeded onto a Collagen R coated surface and lysed using a hot lysis protocol 4 hours later. **(A)** Solo, pY416-Src (pSrc) and Src were normalized to GAPDH (1). pY118-Paxillin (pPaxillin) and Paxillin were normalized to GAPDH (2). **(B)** Signal normalized to shNT shown as bars. (n=1)

4.6 shSolo MDA-MB-231 cells showed decreased total Paxillin and Y118 phosphorylated Paxillin at the FAs

As it was previously observed, Paxillin MFI at the FAs was increased for transient Solo depletion in MDA-MB-231 cells – **Figure 5**. To test whether this effect is conserved for the stable MDA-MB-231 cells, the same experimental setup was used. Stable MDA-MB-231 cells were doxycycline-induced for 72 hours. Cells were seeded onto Collagen R coated coverslips for 4 hours and later fixed, permeabilized and stained for Paxillin. Paxillin was then quantified at the FAs, each value representing the MFI of one isolated FA.

shSolo MDA-MB-231 cells appeared to have more and longer FAs, but with a slightly weaker signal intensity for Paxillin. Additionally, signal intensity for cytosolic Paxillin appeared to be stronger for shNT cells - **Figure 10A**. Solo depleted cells showed a decrease in the MFI of Paxillin, from a MFI of 18.854 a.u. for the control shNT cells, to 15.640 a.u. and 13.567 a.u. for the shSolo#2 and shSolo#3 cells, respectively. – **Figure 10B**.

Since Paxillin is a downstream target of Src (Theocharis *et al.* 2017), it would be expected that phosphorylation levels of this protein at FAs would be decreased upon altered Src localization. To test whether Solo depletion in stable cells alters Paxillin phosphorylation levels at the FAs, an anti-Y118 antibody was used and the MFI at the FAs was assessed by immunofluorescence. Thus, stable MDA-MB-231 cells were doxycycline-induced for 72 hours. Cells were seeded onto Collagen R coated coverslips for 4 hours, and later fixed, permeabilized and stained for pY118 Paxillin. Phosphorylated Paxillin was then quantified at the FAs, each value representing the MFI of one isolated FA.

shSolo MDA-MB-231 cells appeared to have less phosphorylated Paxillin at the FAs. Additionally, signal intensity for cytosolic phosphorylated Paxillin appeared to be stronger for shNT cells – **Figure 10C**. Solo depleted cells showed a decreased MFI for Y118 phosphorylated Paxillin, with a MFI of 1.913 a.u. and 1.660 a.u. for the shSolo#2 and shSolo#3 cells, respectively, in contrast to the MFI of 2.280 a.u. for the control shNT cells - **Figure 10D**.

In summary, and in agreement to what was observed for the transient Solo depleted cells, shSolo MDA-MB-231 cells showed longer FAs. On the other hand, in concordance to what was expected, Paxillin phosphorylation was decreased in Solo depleted cells.

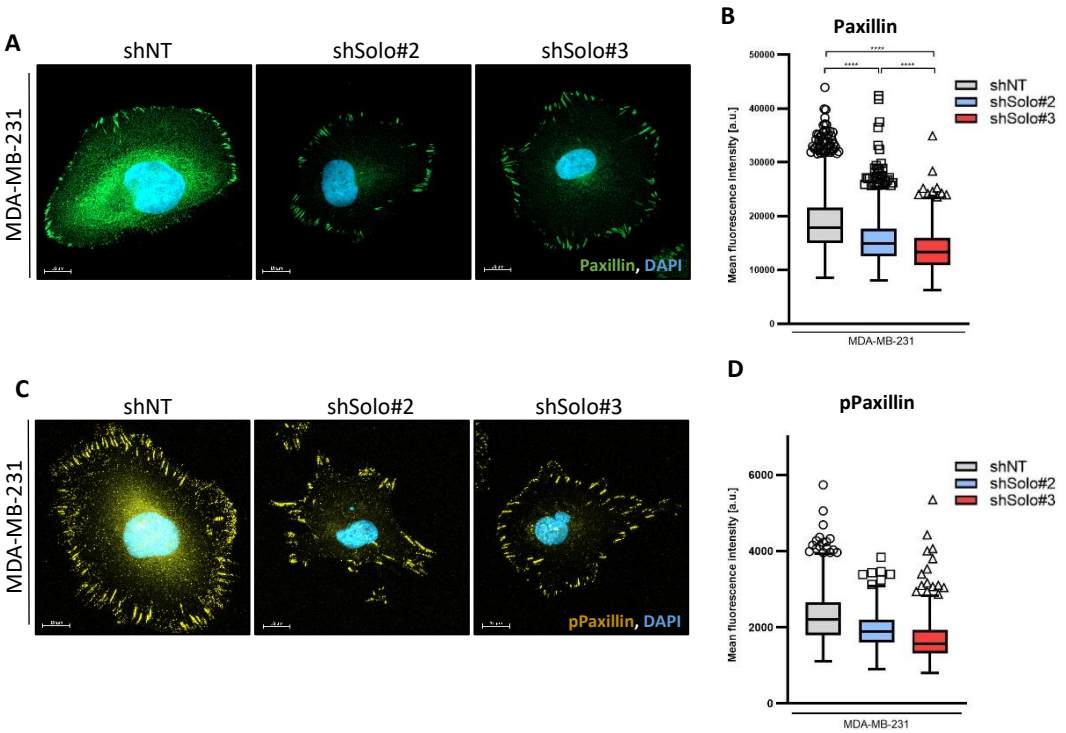

Figure 10. **Paxillin and pPaxillin are reduced in stable shSolo MDA-MB-231 cells. (A, D)** Stable MDA-MB-231 cells were doxycycline-induced for 72 hours. 8.300 cells·cm^{-2} were seeded onto Collagen R coated coverslips, fixed 4 hours later, stained for Paxillin (green) or pPaxillin (yellow) and DNA counterstained with DAPI (blue). **(A, C)** The images are maximum intensity projections of several confocal sections. Scale bars: 10µm. **(B, D)** The mean fluorescence intensity of Paxillin and pPaxillin at focal adhesions in stable MDA-MB-231 cells was assessed and plotted in a tukey-boxplot. Brown-Forsythe and Welch ANOVA comparison tests for each cell line were performed. (n=2; N=16 (shNT), 18 (shSolo#2, shSolo#3) for Paxillin and n=1; N=9 (shNT), 8 (shSolo#2, shSolo#3) for pPaxillin)

4.7 shSolo MDA-MB-231 cells showed an increase in perinuclear Src

Regarding the previous results on Src subcellular distribution, to test whether Solo knock down affects Src localization in the shSolo MDA-MB-231 cells, the subcellular distribution of this protein was assessed by immunofluorescence. Thus, stable MDA-MB-231 cells were doxycycline-induced for 72 hours. Cells were seeded onto Collagen R coated coverslips for 4 hours, and later fixed, permeabilized and stained for Src.

shNT MDA-MB-231 cells appeared to have a homogeneous distribution of Src across the cytoplasm. However, for the shSolo MDA-MB-231 cells, Src accumulations were observed at the perinuclear region and Src signal appeared to be less intense at the plasma membrane – **Figure 11**. In conclusion, and similarly to what was previously observed for transient Solo depletion in parental MDA-MB-231 cells, Src also accumulates at the perinuclear region in shSolo stable MDA-MB-231 cells.

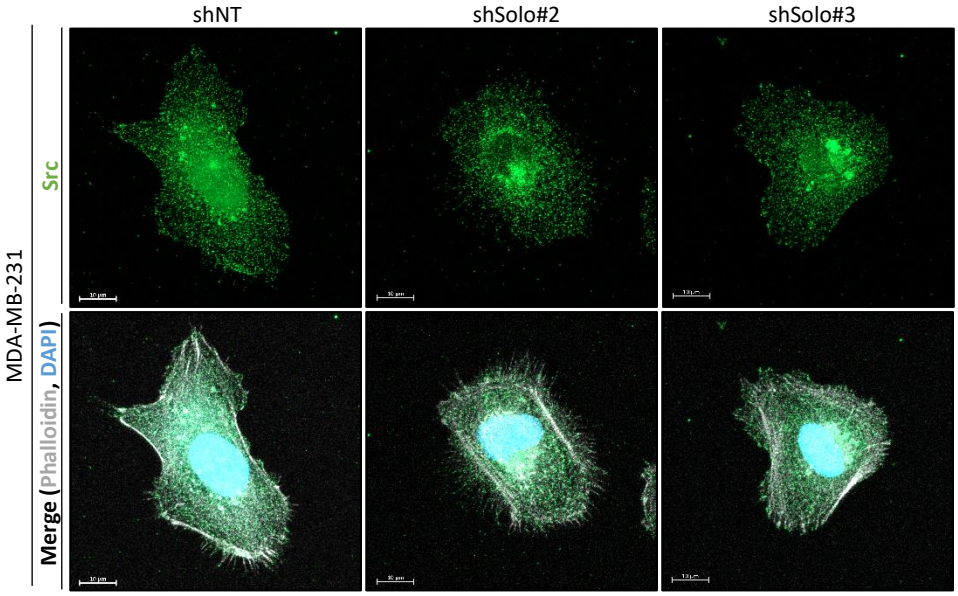

Figure 11. Src accumulates at the perinuclear region upon Solo knock down in stable cells. Stable MDA-MB-231 cells were doxycycline-induced for 72 hours. 8.300 cells·cm^{-2} were seeded onto Collagen R coated coverslips, fixed 4 hours later and stained for Src (green), actin stained with Alexa Fluor-633 labelled Phalloidin (white) and DNA counterstained with DAPI (blue). The images are maximum intensity projections of several confocal sections. Scale bars: 10µm. (n=2; N=16 (shNT), 18 (shSolo#2, shSolo#3)

4.8 Overall tyrosine residues were relatively less phosphorylated in FAs in shSolo MDA-MB-231 cells

Src activity is known to affect not only FAs size but also phosphotyrosine levels at these sites (Wu *et al.* 2015). Because Src accumulated at the perinuclear region upon Solo knock down, it was hypothesized that decreased levels of Src at FAs would come along with decreased phosphotyrosine levels at FAs. To assess phosphotyrosine levels at the FAs upon Solo depletion, stable MDA-MB-231 cells were doxycycline-induced for 72 hours. Cells were seeded onto Collagen R coated coverslips for 4 hours, and later fixed, permeabilized and stained for phosphotyrosine. Phosphotyrosine was then quantified at the FAs, each value representing the MFI of one isolated FA

Solo depleted cells presented less intense phosphotyrosine signal at the FAs, when compared to the shNT MDA-MB-231 cells - **Figure 12A**. shNT MFI presented higher values, surpassing 40.000 a.u. For all shNT, shSolo#2 and shSolo#3 cells two populations of MFI were observed: highly phosphorylated population with higher MFI values, and a less phosphorylated one, with lower MFI values- **Figure 12B**. To better observe the latter population the cut-off was set to 10.000 a.u., which was close to the median values and thus including approximately 50% of the total values. Of this lower population, shNT cells showed a MFI median 5.439 a.u. while shSolo#2 and shSolo#3 cells showed a decreased MFI median of 4.603 a.u. and 4.383 a.u., respectively – **Figure 12C**. Overall, these results demonstrate that, as it was hypothesized, FAs in shSolo MDA-MB-231 cells show a reduced phosphotyrosine signal, indicating altered FA signaling. The decreased FA phosphorylation could indicate that, due to the mislocalization of Src upon Solo knock down, the kinase activity of Src might be altered at the FAs. Thus, Solo might affect Src localization and activity. For this reason, it would be worth investigating whether Solo affects Src localization in a 3D model as well.

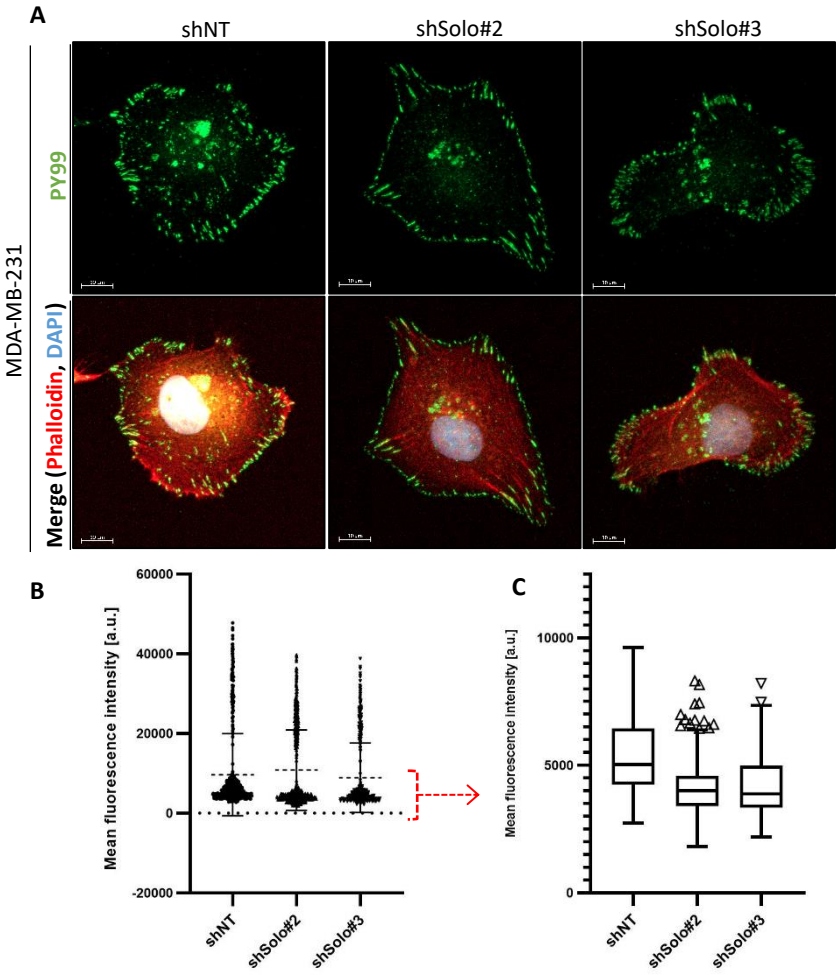

Figure 12. Phosphotyrosines at focal adhesions are reduced in shSolo stable MDA-MB-231 cells. Stable shSolo MDA-MB-231 cells were doxycycline-induced for 72 hours. 8.300 cells·cm^{-2} were seeded onto Collagen R coated coverslips, fixed 4 hours later and phosphotyrosine stained with PY99 (green), DNA counterstained with DAPI (blue) and actin stained with Alexa Fluor-633 Phalloidin (red). **(A)** The images are maximum intensity projections of several confocal sections. Scale bars: 10µm. **(B)** The MFI of PY99 at focal adhesions was assessed and plotted in a tukey-boxplot. **(C)** Zoom-in on the population of MFI values below 10.000 a.u. of phosphotyrosine at the focal adhesions of stable MDA-MB-231 cells from (B). (n=1; N=9 (shNT, shSolo#3), 8 (shSolo#2))

4.9 Src showed a decrease intra and extracellularly in 3D spheroids for shSolo MDA-MB-231 cells

Cultured tumor cells in 3D microenvironments have consistent protein expression differences when compared to flask-cultured cells (Kenny *et al*. 2007). As shown before, Src localization was affected by Solo depletion when cells were cultured two dimensions – **Figure 11**. To test whether this behavior is conserved in a 3D microenvironment, stable cells were doxycycline-induced for 72 hours and seeded in a 1:1 Matrigel/Collagen bed. After 7 days, cells were fixed and stained for Src.

Stable cells were able to form spheroids in a mass-like morphology, with non-polarized nuclei and robust cell-cell adhesions. Some spheroids appeared to have membrane extensions to the extracellular matrix (ECM) while others seemed to have a more spherical and robust structure. However, regarding spheroid morphology, differences between control and shSolo cells were not observed. Src seemed to be more abundant in shNT cells and to accumulate stronger in the extracellular regions of the formed spheroids than for shSolo cells– **Figure 13A**. Images from one confocal section from the middle of the spheroids also showed Src to be generally reduced intracellularly and at cell-cell contacts upon Solo depletion – **Figure 13B**. Overall, these results indicate that the morphology of the stable cell spheroids doesn't change between shSolo and control cells and that, for the latter, Src levels are generally decreased.

In summary, Solo knock down in MDA-MB-231 cells resulted in the accumulation of Src at the perinuclear region. Additionally, Solo depletion resulted in overall decrease of tyrosine phosphorylation at FAs as well as decreased Y118 phosphorylation of the FA resident scaffolding protein Paxillin at FAs. Moreover, FAs showed an enlargement in both siSolo and shSolo cells. Finally, the knock down of that RhoGEF protein resulted in the decrease of Src in 3D culture. Considering this, it would be of great interest to understand the role of Solo in FA development and, as a result, in cell migration.

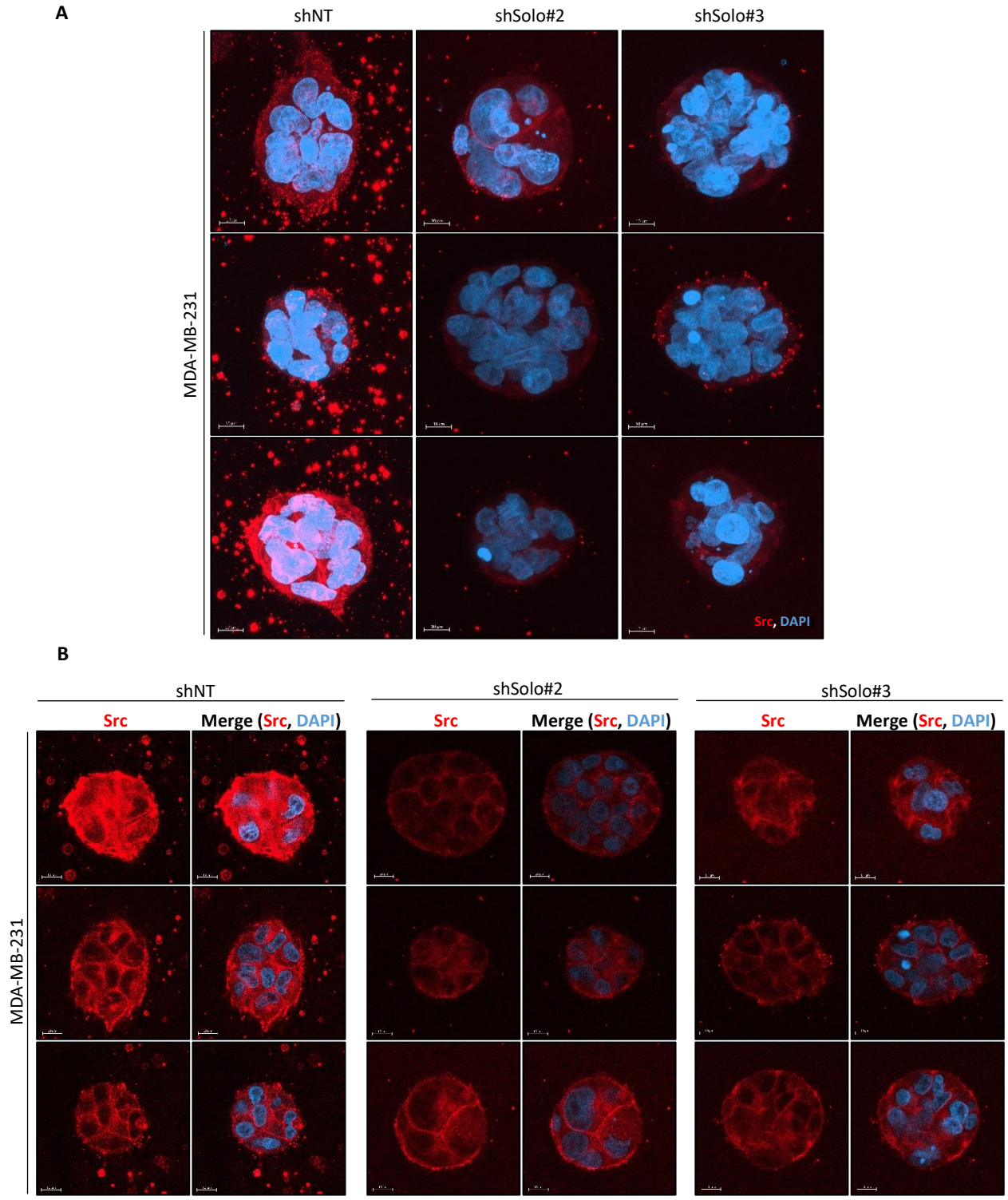

Figure 13. Extracellular and total Src are decreased for shSolo MDA-MB-231 spheroids in 3D conditions. (A, B) Immunofluorescence of stable MDA-MB-231 cells. Cells were doxycycline-induced for 72 hours. 1.429 cells·cm^{-2} were seeded on top of a 1:1 Matrigel/Collagen bed. After 7 days cells were fixed and stained for Src (red) and DNA counterstained with DAPI (blue). **(A)** The images are maximum intensity projections of several confocal sections. **(B)** The images are one confocal section from the middle of the spheroid. Scale bars: 10µm. (n=1)

5. Discussion

Triple-negative breast cancer (TNBC) is clinically characterized as the most aggressive and least responsive to standard treatment of all breast cancer (BC) subtypes. Furthermore, patients with TNBC have an increased likelihood of distant recurrence, as compared to those with non-TNBC subtypes (Singh *et al.* 2021, Neophytou *et al.* 2018). In fact, metastases are the leading cause of BC death, not the primary tumor. During metastasis, cancer cells undergo shape changes, a process regulated by Rho GTPases (Pascual-Vargas *et al.* 2017). The RhoGEF protein Solo plays an important role in TNBC cell motility (Florian Meyer, unpublished data). In this thesis, the effects of Solo knock down in TNBC cells focal adhesions (FAs) development and Src trafficking were assessed by immunofluorescence.

5.1 Solo regulates Src localization and activity in stable MDA-MB-231 cells

The accumulation of Src at the perinuclear region upon Solo depletion in stable MDA-MB-231 cells – **Figure 11** – suggests that this kinase trafficking could be regulate by this RhoGEF. As a matter of fact, Src is known to be translocated in between the perinuclear region and the cell membrane in a RhoB-dependent manner (Reinecke and Caplan 2014) and Solo was discovered to regulate both RhoB-GTP and total RhoB levels in HeLa cells (Lungu *et. al* 2022). Taking this into account, in Solo depleted cells RhoB would be reduced. As a consequence, the translocation of active Src to the cell periphery would be impaired. In fact, the RhoGEF protein GEF-H1, known to activate RhoB, was previously identified to facilitate the bimodal transport of Src in human epithelial cells. Here, GEF-H1-dependent RhoB activation was observed to coordinate both microtubuli and actine polymerization, necessary mechanisms for efficient trafficking of Src-associated endosomes (Arnette *et al.* 2016). Thus, the observed Src localization at the perinuclear region could be explained by its inability to get translocated to the FAs. In addition, to test if RhoB activity levels are changed, a Rho-binding domain (RBD) pulldown could be performed or, as an alternative, a spatiotemporal monitorization of its activity by using a RhoB biosensor. Interestingly, changes in Src localization might indicate alterations in its activity.

Reduced Src activity in shSolo cells – **Figure 9** – further endorses the hypothesis that Solo might regulate Src trafficking. In fact, Src activity is determined by its subcellular localization (Simatou *et al.* 2020). While inactive Src is found at the perinuclear region, active Src localizes to the FAs (Reinecke and Caplan 2014). For this reason, cells showing an accumulation of Src at the perinuclear region – **Figure 11** – would be anticipated to show less active Src as well. In spite of this, increased Src activity in siSolo transfected cells – **Figure 7** – would suggest otherwise. However, it is worth noting that viscous cell lysates were observed upon hot lysis of these cells, possibly resulting from DNA abundance in the samples, as it is known to increase viscosity in cell lysates (Menacho-Melgar and Lynch 2022). To overcome this problem, passing the lysate through a needle via syringe or adding DNase to the lysate could help in reducing viscosity. It should also be noted that through western blotting it is not possible to learn the protein subcellular localization. Thus, a possible decrease in localized Src activity would not be able to be detected through western blot if the activity of this protein increased elsewhere in the cell. In addition, the used antibody detects all Src-family kinases (SFKs) phosphorylated at the Y416 residue. Given that SFKs are comparable or identical in molecular weight, Src phosphorylation levels could be masked by the phosphorylation of other SFK proteins. In fact, other SFK proteins were also observed to be overexpressed in BC as it is the case for Fyn (Xie *et al.* 2016) and Yes (Bilal *et al.* 2010). Hence, Src could be isolated through immunoprecipitation and phosphorylated Src analyzed for a more precise understanding of Src activity. Finally, Src activity was quantified only once, thus further experimental repetitions should be performed. Of note, perinuclear accumulations of Src in siSolo transfected BT549 cells were not observed – **Figure 6**. Nevertheless, since Src activity was found to be reduced in western blot upon Solo depletion – **Figure 7** – this data suggests that Solo could regulate Src activity in BT549 cells as well.

In summary, this data provides first indications that Solo could regulate Src trafficking in MDA-MB-231 cells. However, it's unclear whether Src activation is impaired upon Solo knock down, or if Src inactivation is affected. Considering Src dual localization, under non-stimulated conditions the vast majority of this kinase is found at the perinuclear region and was observed to localize to endosomes in mammalian fibroblasts (Kaplan *et al.* 1992). Src is also often found on RhoB decorated vesicles. Sandilands *et al.* provided the first direct evidence that Src translocation is directly regulated by endosomes. In fact,

recycling endosomes were observed to be crucial for Src translocation to the cell periphery, considering that this kinase was retained at these endosomes by inhibiting their trafficking. Additionally, data also suggests that Src trafficking can be regulated by late endosomes (LEs) and lysosomes in HeLa cells. Furthermore, RhoB was observed to be able to regulate endosome motility along the actin cytoskeleton by recruiting the protein mDia1 (Reinecke and Caplan 2014). RhoB was also shown to localize to LEs and to be necessary for Src delivery to the cell periphery, indicating that Src trafficking in between the perinuclear region and the cell periphery occurs in a RhoB-dependent manner (Tu *et al.* 2010). To further investigate the possibility of the Solo-RhoB axis having a role in Src trafficking, colocalization studies of these proteins could be performed in TNBC cell lines. Considering its localization, Reinecke and Caplan suggested that active Src at the plasma membrane might be ubiquitinated and transported to late endosomal-lysosomal compartment for degradation. Additionally, they also suggested that active Src might be recycled to the perinuclear endocytic recycling compartment (ERC), in which it is unable to coordinate downstream signaling events, necessary for cell motility and migration (Reinecke and Caplan 2014). To further test these questions, the co-localization of Src with known organelle markers such as Rab5 (EE), Rab7 (LE) and Rab11 (recycling endosome) could be investigated (Sandilands *et al.* 2004). Considering this data, it would be expected that this Src accumulation might be a result of recycled Src, possibly internalized through endocytosis. The observed accumulated perinuclear Src in shSolo cells might localize to recycling endosomes, thus Src is expected to co-localize with the recycling endosome marker Rab11.

5.2 Solo regulates Src downstream signaling

Impaired Src trafficking to the FAs and reduced Src activity might explain the reduction of overall tyrosine phosphorylation at the FAs, shown by pY-staining and phosphorylated Paxillin, in shSolo cells – **Figure 12** and **Figure 10D**, respectively. In fact, it is known that the phosphorylation of Src-downstream substrates, such as Paxillin and FAK, requires Src at the FAs (Wu *et al.* 2015). As a consequence of such trafficking impairment, this kinase wouldn't be able to interact and phosphorylate its targets at the FAs. Reduced phosphotyrosine levels were previously observed in cells lacking the SFKs Src, Yes and Fyn ($SYF^{-/-}$ cells) (Cary *et al.* 2002). Furthermore, tyrosine phosphorylation

at the FAs is necessary for cell migration (Wu *et al*. 2015). Hence, as a consequence of decreased tyrosine phosphorylated proteins, it would be expected that cell migration would decrease in Solo depleted cells, as it previously was observed for the $SYF^{-/-}$ cells (Cary *et al.* 2002). In fact, a decrease in cell motility was also observed for the MDA-MB-231, BT549 and HS578T cell lines upon transient Solo depletion in our laboratory (Florian Meyer, unpublished data). In short, impaired Src trafficking might result in changed cellular motility behavior through the overall tyrosine phosphorylation at the FAs.

As a downstream effector of Src (Noh *et al.* 2021), the adaptor protein Paxillin as a major component of FAs (Dong *et al.* 2009) was also investigated upon Solo depletion. Paxillin was observed to be more phosphorylated in siSolo transfected MDA-MB-231 and BT549 cells, as well as shSolo MDA-MB-231 cells – **Figure 7** and **Figure 9**, respectively – indicating that Solo depletion leads to an increased phosphorylation of this protein. However, it should be noted that FAK is critical to the Y118 Paxillin phosphorylation (Pasapera *et al.* 2010), as this protein recruits Src to the FAs upon autophosphorylation (Sachdev *et al.* 2009). Thus, the phosphorylation levels of Paxillin at Y118 are a result not just of Src but also FAK activity. Additionally, through western blotting it is not possible to understand in which subcellular region the phosphorylation is changed. For that matter, through immunofluorescence, it was possible to observe a reduction in phosphorylated Paxillin at the FAs in the cell periphery – **Figure 10D** – indicating that phosphorylated Paxillin might be present in higher levels in shSolo cells in other subcellular locations. It should be noted that FAs anchor stress fibers not only at the cell periphery but in other regions of the cell as well. Wirtz *et al.* identified a subset of ventral stress fibers, actin cap associated FAs (ACAFAs), that wrap over the nucleus, being involved in the nucleus shape remodeling during migration (Burridge *et al.* 2016). ACAFAs were identified to be larger than conventional FAs, possibly as a result of being under more pressure presumably caused by the nucleus exercised pressure. Additionally, ACAFAs were found to have significantly higher levels of the FA-associated protein Vinculin (Kim *et al.* 2012). In addition, adhesions formed between the integrin receptors and the extracellular matrix (ECM) can mature into Focal complexes (FXs) that localize away from the leading edge, at the border between the lamellipodia and the lamella (Galbraith *et al.* 2002). Interestingly, FXs were observed to be associated with tyrosine-

phosphorylated Paxillin (Zaidel-Bar *et al.* 2007). Considering this, higher phosphorylated Paxillin levels in such FA populations could explain why overall Paxillin phosphorylation increases, even if it decreases at the cell periphery. Since Solo knock down could result in a FAs population switch, apart from the FAs at the cell periphery, other FAs should be investigated as well.

Higher mean fluorescence intensity (MFI) of Paxillin at the FAs in both siSolo transfected MDA-MB-231 and BT549 cells – **Figure 5** – could indicate that FAs stabilization occurs upon Solo depletion. These observations agree with previous results showing that MDA-MB-231 and BT549 cells present lower motility upon siRNA mediated Solo knock down (Florian Meyer, unpublished data). Unexpectedly, shSolo MDA-MB-231 cells showed a decreased MFI for Paxillin at the FAs, which would indicate FAs to be less stable – **Figure 10B**. However, it should be noted that shSolo MDA-MB-231 cells seemed to exhibit longer FAs – **Figure 10A**. To understand if this was the case, FAs area or length-to-width ratio were calculated. However, differences were not observed upon Solo depletion (data not shown) possibly due to quantification limitations that this method holds. Considering the high number of FAs present in every cell, an automated quantification was chosen in order to uniformize the quantifications. However, certain single FAs were detected as multiple FAs (and vice-versa). Thus, through this methodology, the length of single FAs could not be accurately determined as well. To gain further insights, Paxillin dynamics and FAs size could be followed by Total Internal Reflection Fluorescence Microscopy (TIRF) as a high-resolution analysis for FAs spatiotemporal dynamics in living cells, more specifically, FAs location, size, shape, and signal intensity (Berginski *et al.* 2011), by following fluorescent tagged Paxillin. Lastly, Fluorescence Recovery After Photobleaching (FRAP) could also be performed in order to study Paxillin mobility at the FAs in living shSolo cells. Through FRAP it would be possible to understand whether Paxillin mobility at the FA is rapid or slow and how stable immobile fractions are. Additionally, cell motility could be altered in shSolo cells as well. For that reason, a random motility assay could be performed, with the purpose to understand if shSolo cell velocity is altered as a consequence of altered FAs size.

Interestingly, phosphorylated and total Paxillin were also observed to be decreased in the cytosol in shSolo MDA-MB-231 cells – **Figure 10A** and **Figure 10C**, respectively – suggesting that Solo might affect the function of Paxillin not only at the FAs. In fact,

Paxillin was found to localize at the cytosol and to affect gene transcription (Hu *et al.* 2014, Dong *et al.* 2009). The first evidence of this was observed in fibroblasts, in which Paxillin interacts with the mRNA binding protein polyadenylation binding protein 1 (PABP1). These proteins co-localized in the endoplasmic reticulum and in the nucleus. This association was observed to facilitate mRNA transport from the nucleus to protein synthesis sites at the leading-edge (Ma and Hammes 2018). In turn, this was observed to be necessary not only for FA remodeling but also for cell migration (Woods *et al.* 2005). Considering this data, Solo might also have an effect in cytosolic Paxillin distribution and, consequently, FAs development. This altered distribution could be mediated by the phosphorylation of the cytosolic Paxillin fraction, possibly as a result of altered Src localization and activity. To test whether the aberrant Paxillin localization upon Solo knock down is indeed mediated by aberrant Src localization/activity, Paxillin localization could be investigated in Src knock down MDA-MB-231 cells.

5.3 Src localization is affected by Solo depletion in 3D spheroids

In a three-dimensional (3D) Matrigel/collagen bed Src localization was also affected by Solo depletion in stable MDA-MB-231 cells – **Figure 13**. Notably, decreased Src levels in the shSolo MDA-MB-231 cell spheroids – **Figure 13B** – could indicate that Solo might play a role in this kinase activity, resulting in its altered turnover. Src is known to be hyperactive in many cancers (Reinecke and Caplan 2014). Furthermore, Src was shown to be degraded in a ubiquitin-dependent manner and that active Src is specifically targeted for degradation (Tanaka *et al.* 2020), possibly considering that this form is less stable than the inactive kinase (Harris *et al.* 1999). Besides this, RhoB was shown to be necessary for Src activation in RhoB-null fibroblasts (Sandilands *et al.*2004). Thus, in shSolo cells, active Src could be degraded through the aforementioned mechanism but the activation of inactive Src would be strongly impaired as a result of inactive RhoB. According to what was previously hypothesized, this inactive Src would be expected to be accumulated at the perinuclear region in recycling endosomes. In fact, vesicle-associated RhoB was observed to regulate Rab11-mediated recycling endosomes of the integrin LFA-1 to the cell surface, as the impairment of RhoB function resulted in the accumulation of both Rab11 and LFA-1 (Samuelsson *et al.* 2017). Hence, Src activity would be reduced and total Src levels would be expected to be increased as a consequence. Unexpectedly,

considering the decrease in total Src levels, this is not the case. However, shSolo cells might have multiple biological pathways altered, possibly affecting the secretome.

As an example of the effects of Solo knock down in 3D cultured MDA-MB-231 cells, the composition of the ECM could be altered. In fact, Görtzen *et al.* observed that hepatocytes cultured in higher stiffness gels showed increased Src transcription levels when compared to cells cultures in less rigid conditions (Görtzen *et al.* 2015). Considering that the RhoA/ROCK-mediated signaling is associated with the remodeling and the assembly of ECM components, such as fibronectin (Yodoi *et al.* 2009), it is also possible that the knock down of Solo, a RhoA-targeting protein (Lungu *et al.* 2022), results in the alteration of the ECM architecture. In fact, the knock down of Solo in TGF-β treated MCF10A cells was observed to lead to an increase in fibronectin expression and deposition in a two-dimensional (2D) microenvironment (Florian Meyer, unpublished data). Thus, it is possible that both the secretion and remodeling via RhoA might be changed in 3D as well. To understand if Src transcription levels are also altered in the MDA-MB-231 cell line as a consequence of the ECM stiffness and Solo knock down, Src mRNA levels could be investigated in cells seeded under different stiffness conditions. To reveal possible alterations in the ECM components as a result of Solo knock down, a mass spectrometry-based proteomics approach could be followed.

In 3D conditions shSolo MDA-MB-231 cells show decreased extracellular Src – **Figure 13A**. The observed extracellular Src might be vesicles such as exosomes. In fact, Franchi *et al.* demonstrated that MDA-MB-231 cell grown in 3D conditions show an increase in exosomes and microvesicles (Franchi *et al.* 2020). Src could be involved in the regulation of their secretion. Tanaka *et al.* reported that, in order to decrease activated Src levels, ubiquitination of Src preferentially promotes its secretion via extracellular vesicles in MDCK cells. In this study, an accumulation of ubiquitinated Src at Lys429 upon the inhibition of the proteosome pathway was not observed. These results suggest that Src ubiquitination promotes preferentially its secretion in order to decrease activated Src in MDCK cells. However, such studies have not yet been performed in cancer cells (Tanaka *et al.* 2020). For that matter, studying Src behavior upon treating cells with a proteasome inhibitor, such as MG132 (Tanaka *et al.* 2020), could help understand if the previous results for the MDCK cells are also observed in MDA-MB-231 cells. In addition, the inhibition of Src activity was observed to result in reduced exosome secretion by chronic

myeloid leukemia cells and to reduce the ability of exosomes to stimulate Human umbilical vein endothelial cells (HUVEC) migration (Imjeti *et al.* 2017). Thus, a reduction in extracellular and intracellular Src in Solo depleted MDA-MB-231 cells – **Figure 13A** - could indicate that changes of total levels of Src have an impact on exocytosis.

As it is the case for the MDA-MB-231 cell line and in various cancers, exosomes are shown to be Src enriched. These exosomes can be uptaken by neighboring cancer cells, allowing them to acquire intercellular protrusions, and providing direct communication and molecular exchange between cells (Franchi *et al.* 2020, Simatou *et al*. 2020). For example, Src-containing vesicles from MDA-MB-231 cells are known to induce cell migration and invasion in a Src-dependent pathway (Ramírez-Ricardo *et al.* 2020). Consequently, decreased Src-containing exosomes upon knock down of Solo could result in reduced activation of Src-dependent pathways in neighboring cells. As a result, cell migration and invasion would not be induced through this mechanism. To clarify whether Src-dependent mechanisms could be altered as a result of decreased Src-containing vesicles, parental cells could be treated with the supernatant of control or shSolo MDA-MB-231 cells. The cell lysis of the treated cells could be followed by a phosphoproteomic approach, enabling the analysis of up- and downregulated pathways.

5.4 Outlook

In this thesis the depletion of Solo in stable MDA-MB-231 cells was shown to result in Src accumulation at the perinuclear region. These observations were also confirmed in siSolo transfected MDA-MB-231 cells – **Figure 6**. In 3D this kinase was also observed to have an altered localization. As Src is known to be overexpressed in most BC patients, including MDA-MB-231 cell lines (Kwak *et al.* 2019), as well as Solo (David Benz, unpublished data), the interplay of these two proteins might play a major role in TNBC cells behavior. In fact, Solo was recently shown to interact and to be phosphorylated by Src (Florian Meyer, unpublished data). Considering that both proteins are connected to RhoB-positive endosomes (Lungu *et. al* 2022, Reinecke and Caplan 2014) it is possible that the activity of Src might be necessary for Solo activation. Given that many other proteins are transported on RhoB-positive endosomes (Fernandez-Borja *et al.* 2005) it

will be an interesting task to identify additional pathways that are perturbed due to this axis.

The experiments performed during this thesis had a main focus on the MDA-MB-231 cells. However, considering that stable BT549 and HS578T were also generated, investigating the role of Solo in Src trafficking and FA development in these two TNBC cells would also help to understand if these effects are conserved in the mentioned BC cell lines. Furthermore, Src could be fluorescently labeled and its trafficking followed in the generated shSolo cells as well.

Exploring the role of Solo in TNBC would be crucial to better comprehend the biological processes that tumor cells undergo so that distant metastasis occurs. Considering this subgroup to be the most aggressive and the most likely to form metastasis (Singh *et al.* 202), understanding the mechanisms in which Solo is involved could provide promising scientific input and alternative treatments for BC patients.

This page was intentionally left blank.

References

Adini, I., Rabinovitz, I., Sun, J. F., Prendergast, G. C., & Benjamin, L. E. (2003). RhoB controls Akt trafficking and stage-specific survival of endothelial cells during vascular development. *Genes and Development*, *17*(21), 2721–2732. https://doi.org/10.1101/gad.1134603

Ampe, C. (2016) Mammalian actions: Isoform-specific functions and diseases. In J. Brigitte (Ed.) *The actin cytoskeleton* (pp 1-37). Switzerland: Springer.

Arnette, C., Frye, K., & Kaverina, I. (2016). Microtubule and actin interplay drive intracellular c-Src trafficking. *PLoS ONE*, *11*(2). https://doi.org/10.1371/journal.pone.0148996

Badea, M. A., Balas, M., Hermenean, A., Ciceu, A., Herman, H., Ionita, D., & Dinischiotu, A. (2019). Influence of Matrigel on Single- and Multiple-Spheroid Cultures in Breast Cancer Research. *SLAS Discovery*, *24*(5), 563–578. https://doi.org/10.1177/2472555219834698

Berginski, M. E., Vitriol, E. A., Hahn, K. M., & Gomez, S. M. (2011). High-resolution quantification of focal adhesion spatiotemporal dynamics in living cells. *PLoS ONE*, *6*(7). https://doi.org/10.1371/journal.pone.0022025

Bilal, E., Alexe, G., Yao, M., Cong, L., Kulkarni, A., Ginjala, V., Toppmeyer, D., Ganesan, S., & Bhanot, G. (2010). Identification of the YESI kinase as a therapeutic target in basal-like breast cancers. *Genes and Cancer*, *1*(10), 1063–1073. https://doi.org/10.1177/1947601910395583

Burridge, K., & Guilluy, C. (2016). Focal adhesions, stress fibers and mechanical tension. *Experimental Cell Research*, *343*(1), 14–20. https://doi.org/10.1016/j.yexcr.2015.10.029

Cary, L. A., Klinghoffer, R. A., Sachsenmaier, C., & Cooper, J. A. (2002). Src Catalytic but Not Scaffolding Function Is Needed for Integrin-Regulated Tyrosine Phosphorylation, Cell Migration, and Cell Spreading. *Molecular and Cellular Biology*, *22*(8), 2427–2440. https://doi.org/10.1128/mcb.22.8.2427-2440.2002

Curtis, C., Hemmeryckx, B., Haataja, L., Senadheera, D., Groffen, J., & Heisterkamp, N. (2004). Scambio, a novel guanine nucleotide exchange factor for Rho. *Molecular Cancer*, *3*, 1–12. https://doi.org/10.1186/1476-4598-3-10

Deakin, N. O., & Turner, C. E. (2008). Paxillin comes of age. *Journal of Cell Science*, *121*(15), 2435–2444. https://doi.org/10.1242/jcs.018044

Dong, J. M., Lau, L. S., Ng, Y. W., Lim, L., & Manser, E. (2009). Paxillin nuclear-cytoplasmic localization is regulated by phosphorylation of the LD4 motif: Evidence that nuclear paxillin promotes cell proliferation. *Biochemical Journal*, *418*(1), 173–184. https://doi.org/10.1042/BJ20080170

El Hachem, G., Gombos, A., & Awada, A. (2019). Recent advances in understanding breast cancer and emerging therapies with a focus on luminal and triple-negative breast cancer. *F1000Research*, *8*. https://doi.org/10.12688/f1000research.17542.1

Eyckmans, J., Boudou, T., Yu, X., & Chen, C. S. (2011). A Hitchhiker's Guide to Mechanobiology. *Developmental Cell*, *21*(1), 35–47. https://doi.org/10.1016/j.devcel.2011.06.015

Fagan-Solis, K. D., Schneider, S. S., Pentecost, B. T., Bentley, B. A., Otis, C. N., Gierthy, J. F., & Arcaro, K. F. (2013). The RhoA pathway mediates MMP-2 and MMP-9-independent invasive behavior in a triple-negative breast cancer cell line. *Journal of Cellular Biochemistry*, *114*(6), 1385–1394. https://doi.org/10.1002/jcb.24480

Fernandez-Borja, M., Janssen, L., Verwoerd, D., Hordijk, P., & Neefjes, J. (2005). RhoB regulates endosome transport by promoting actin assembly on endosomal membranes through Dia1. *Journal of Cell Science*, *118*(12), 2661–2670. https://doi.org/10.1242/jcs.02384

Franchi, M.; Piperigkou, Z.; Karamanos, K.-A.; Franchi, L.; Masola, V. (2020) Extracellular Matrix-Mediated Breast Cancer Cells Morphological Alterations, Invasiveness, and Microvesicles/Exosomes Release. *Cells*,*9*, 2031. https://doi.org/10.3390/cells9092031

Fritz, G., Brachetti, C., Bahlmann, F., Schmidt, M., & Kaina, B. (2002). Rho GTPases in human breast tumours: Expression and mutation analyses and correlation with clinical parameters. *British Journal of Cancer*, *87*(6), 635–644. https://doi.org/10.1038/sj.bjc.6600510

Fu, P., Epshtein, Y., Ramchandran, R., Mascarenhas, J. B., Cress, A. E., Jacobson, J., Garcia, J. G. N., & Natarajan, V. (2021). Essential role for paxillin tyrosine phosphorylation in LPS-induced mitochondrial fission, ROS generation and lung endothelial barrier loss. *Scientific Reports*, *11*(1). https://doi.org/10.1038/s41598-021-97006-y

Fujiwara, S., Matsui, T. S., Ohashi, K., Deguchi, S., & Mizuno, K. (2018). Solo, a RhoA-targeting guanine nucleotide exchange factor, is critical for hemidesmosome formation and acinar development in epithelial cells. *PLoS ONE*, *13*(4), 1–17. https://doi.org/10.1371/journal.pone.0195124

Fujiwara, S., Ohashi, K., Mashiko, T., Kondo, H., & Mizuno, K. (2016). Interplay between Solo and keratin filaments is crucial for mechanical forceinduced stress fiber reinforcement. *Molecular Biology of the Cell*, *27*(6), 954–966. https://doi.org/10.1091/mbc.E15-06-0417

Galbraith, C. G., Yamada, K. M., & Sheetz, M. P. (2002). The relationship between force and focal complex development. *Journal of Cell Biology*, *159*(4), 695–705. https://doi.org/10.1083/jcb.200204153

Goh, C. Y., Wyse, C., Ho, M., O'Beirne, E., Howard, J., Lindsay, S., Kelly, P., Higgins, M., & McCann, A. (2020). Exosomes in triple negative breast cancer: Garbage disposals or Trojan horses? *Cancer Letters*, *473*(November 2019), 90–97. https://doi.org/10.1016/j.canlet.2019.12.046

Görtzen, J., Schierwagen, R., Bierwolf, J., Klein, S., Uschner, F. E., van der Ven, P. F., Fürst, D. O., Strassburg, C. P., Laleman, W., Pollok, J. M., & Trebicka, J. (2015). Interplay of matrix stiffness and c-SRC in hepatic fibrosis. *Frontiers in Physiology*, *6*(DEC), 1–9. https://doi.org/10.3389/fphys.2015.00359

Haga, R. B., & Ridley, A. J. (2016). Rho GTPases: Regulation and roles in cancer cell biology. *Small GTPases*, *7*(4), 207–221. https://doi.org/10.1080/21541248.2016.1232583

Harris, K. F., Shoji, I., Cooper, E. M., Kumar, S., Oda, H., & Howley, P. M. (1999). Ubiquitin-mediated degradation of active Src tyrosine kinase. *Proceedings of the National Academy of Sciences of the United States of America*, *96*(24), 13738–13743. https://doi.org/10.1073/pnas.96.24.13738

Hendrick, J., Franz-Wachtel, M., Moeller, Y., Schmid, S., Macek, B., & Olayioye, M. A. (2016). The polarity protein Scribble positions DLC3 at adherens junctions to regulate Rho signaling. *Journal of Cell Science*, *129*(19), 3583–3596. https://doi.org/10.1242/jcs.190074

Hikita, T., Kuwahara, A., Watanabe, R., Miyata, M., & Oneyama, C. (2019). Src in endosomal membranes promotes exosome secretion and tumor progression. *Scientific Reports*, *9*(1), 1–14. https://doi.org/10.1038/s41598-019-39882-z

Hong, T. B., Rahumatullah, A., Yogarajah, T., Ahmad, M., & Yin, K. B. (2010). Potential effects of chrysin on MDA-MB-231 cells. *International Journal of Molecular Sciences*, *11*(3), 1057–1069. https://doi.org/10.3390/ijms11031057

Hu, Y. L., Lu, S., Szeto, K. W., Sun, J., Wang, Y., Lasheras, J. C., & Chien, S. (2014). FAK and paxillin dynamics at focal adhesions in the protrusions of migrating cells. *Scientific Reports*, *4*, 1–7. https://doi.org/10.1038/srep06024

Huang, Z., Yu, P., & Tang, J. (2020). Characterization of triple-negative breast cancer MDA-MB-231 cell spheroid model. *OncoTargets and Therapy*, *13*, 5395–5405. https://doi.org/10.2147/OTT.S249756

Humphries, B., Wang, Z., & Yang, C. (2020). Rho GTPases: Big Players in Breast Cancer Initiation, Metastasis and Therapeutic Responses. *Cells*, *9*(10), 1–22. https://doi.org/10.3390/cells9102167

Imjeti, N. S., Menck, K., Egea-Jimenez, A. L., Lecointre, C., Lembo, F., Bouguenina, H., Badache, A., Ghossoub, R., David, G., Roche, S., & Zimmermann, P. (2017). Syntenin mediates SRC function in exosomal cell-to-cell communication. *Proceedings of the National Academy of Sciences of the United States of America*, *114*(47), 12495–12500. https://doi.org/10.1073/pnas.1713433114

Ingley, E. (2008). Src family kinases: Regulation of their activities, levels and identification of new pathways. *Biochimica et Biophysica Acta - Proteins and Proteomics*, *1784*(1), 56–65. https://doi.org/10.1016/j.bbapap.2007.08.012

Isozaki, Y., Sakai, K., Kohiro, K., Kagoshima, K., Iwamura, Y., Sato, H., Rindner, D., Fujiwara, S., Yamashita, K., Mizuno, K., & Ohashi, K. (2020). The Rho-guanine nucleotide exchange factor Solo decelerates collective cell migration by modulating the Rho-ROCK pathway and keratin networks. *Molecular Biology of the Cell*, *31*(8), 741–752. https://doi.org/10.1091/MBC.E19-07-0357

Jong, B. K., Stein, R., & O'Hare, M. J. (2004). Three-dimensional in vitro tissue culture models of breast cancer - A review. *Breast Cancer Research and Treatment*, *85*(3), 281–291. https://doi.org/10.1023/B:BREA.0000025418.88785.2b

Jovic, M., Sharma, M., Rahajeng, J., & Caplan, S. (2010). The early endosome: A busy sorting station for proteins at the crossroads. *Histology and Histopathology*, *25*(1), 99–112. https://doi.org/10.14670/HH-25.99

Ju, J. A., & Gilkes, D. M. (2018). Rhob: Team oncogene or team tumor suppressor? *Genes*, *9*(2), 1–18. https://doi.org/10.3390/genes9020067

Ju, J. A., Godet, I., DiGiacomo, J. W., & Gilkes, D. M. (2020). RhoB is regulated by hypoxia and modulates metastasis in breast cancer. *Cancer Reports*, *3*(1), 1–13. https://doi.org/10.1002/cnr2.1164

Kalpachidou, T., Spiecker, L., Kress, M., & Quarta, S. (2019). Rho GTPases in the physiology and pathophysiology of peripheral sensory neurons. *Cells*, *8*(6). https://doi.org/10.3390/cells8060591

Kaplan, K. B., Swedlow, J. R., Varmus, H. E., & Morgan, D. O. (1992). Association of p60c-src with endosomal membranes in mammalian fibroblasts. *Journal of Cell Biology*, *118*(2), 321–333. https://doi.org/10.1083/jcb.118.2.321

Karagoz, K., Sinha, R., & Arga, K. Y. (2015). Triple negative breast cancer: A multi-omics network discovery strategy for candidate targets and driving pathways. *OMICS A Journal of Integrative Biology*, *19*(2), 115–130. https://doi.org/10.1089/omi.2014.0135

Keenan, T. E., & Tolaney, S. M. (2020). Role of immunotherapy in triple-negative breast cancer. *JNCCN Journal of the National Comprehensive Cancer Network*, *18*(4), 479–489. https://doi.org/10.6004/jnccn.2020.7554

Kenny, P. A., Lee, G. Y., Myers, C. A., Neve, R. M., Semeiks, J. R., Spellman, P. T., Lorenz, K., Lee, E. H., Barcellos-Hoff, M. H., Petersen, O. W., Gray, J. W., & Bissell, M. J. (2007). The morphologies of breast cancer cell lines in three-dimensional assays correlate with their profiles of gene expression. *Molecular Oncology*, *1*(1), 84–96. https://doi.org/10.1016/j.molonc.2007.02.004

Khaled, N., & Bidet, Y. (2019). New insights into the implication of epigenetic alterations in the EMT of triple negative breast cancer. *Cancers*, *11*(4), 1–21. https://doi.org/10.3390/cancers11040559

Kim, D. H., Khatau, S. B., Feng, Y., Walcott, S., Sun, S. X., Longmore, G. D., & Wirtz, D. (2012). Actin cap associated focal adhesions and their distinct role in cellular mechanosensing. *Scientific Reports*, *2*. https://doi.org/10.1038/srep00555

Koudelková, L., Brábek, J., & Rosel, D. (2021). Src kinase: Key effector in mechanosignalling. *The International Journal of Biochemistry & Cell Biology*, *131*, 105908. https://doi.org/https://doi.org/10.1016/j.biocel.2020.105908

Kwak, S. M., Seo, J., Hwang, J. T., Sung, G. J., Song, J. H., Jeong, J. H., Lee, S. H., Yoon, H. G., Choi, H. K., & Choi, K. C. (2019). EGFR–c-Src-mediated HDAC3 phosphorylation exacerbates invasion of breast cancer cells. *Cells*, *8*(8). https://doi.org/10.3390/cells8080930

Legerstee, K., & Houtsmuller, A. B. (2021). A layered view on focal adhesions. *Biology*, *10*(11). https://doi.org/10.3390/biology10111189

Lehtimäki, J. I., Rajakylä, E. K., Tojkander, S., & Lappalainen, P. (2021). Generation of stress fibers through myosin-driven reorganization of the actin cortex. *ELife*, *10*, 1–43. https://doi.org/10.7554/eLife.60710

Lin, F., Wang, N., & Zhang, T. C. (2012). The role of endothelial-mesenchymal transition in development and pathological process. *IUBMB Life*, *64*(9), 717–723. https://doi.org/10.1002/iub.1059

Liu, A. X., & Prendergast, G. C. (2000). Geranylgeranylated RhoB is sufficient to mediate tissue-specific suppression of Akt kinase activity by farnesyltransferase inhibitors. *FEBS Letters*, *481*(3), 205–208. https://doi.org/10.1016/S0014-5793(00)02003-2

López-Colomé, A. M., Lee-Rivera, I., Benavides-Hidalgo, R., & López, E. (2017). Paxillin: A crossroad in pathological cell migration. *Journal of Hematology and Oncology*, *10*(1), 1–15. https://doi.org/10.1186/s13045-017-0418-y

Lou, Y., Jiang, Y., Liang, Z., Liu, B., Li, T., & Zhang, D. (2021). Role of RhoC in cancer cell migration. *Cancer Cell International*, *21*(1), 1–16. https://doi.org/10.1186/s12935-021-02234-x

Lungu, C., Meyer, F., Hörning, M., Steudle, J., Braun, A., Noll, B., Benz, D., Fränkle, F., Schmid, S., Eisler, S., Olayioye, M. (2022). The GEF-GAP pair Solo and DLC3 balances Rho activity during endocytic transport. https://doi.org/10.1101/2022.03.01.482527

Ma, X., & Hammes, S. R. (2018). Paxillin actions in the nucleus. *Steroids*, *133*, 87–92. https://doi.org/10.1016/j.steroids.2017.10.012

Menacho-Melgar, R., & Lynch, M. D. (2022). Measuring Oligonucleotide Hydrolysis in Cellular Lysates via Viscosity Measurements. *Bio-Protocol*, *12*(2), 10–15. https://doi.org/10.21769/BioProtoc.4304

Mosaddeghzadeh, N., & Ahmadian, M. R. (2021). The rho family gtpases: Mechanisms of regulation and signaling. *Cells*, *10*(7). https://doi.org/10.3390/cells10071831

National Cancer Institute (2021). TCGA-BRCA. GDC Data Portal. NCI. https://portal.gdc.cancer.gov/projects/TCGA-BRCA

Nedeljković M, Damjanović A. (2019) Mechanisms of Chemotherapy Resistance in Triple-Negative Breast Cancer—How We Can Rise to the Challenge. *Cells*. 8(9):957. https://doi.org/10.3390/cells8090957

Neophytou, C., Boutsikos, P., & Papageorgis, P. (2018). Molecular mechanisms and emerging therapeutic targets of triple-negative breast cancer metastasis. *Frontiers in Oncology*, *8*(FEB). https://doi.org/10.3389/fonc.2018.00031

Nicolini, A., Ferrari, P., & Biava, P. M. (2021). Exosomes and cell communication: From tumour-derived exosomes and their role in tumour progression to the use of exosomal cargo for cancer treatment. *Cancers*, *13*(4), 1–24. https://doi.org/10.3390/cancers13040822

Nishimura, R., Kato, K., Fujiwara, S., Ohashi, K., & Mizuno, K. (2018). Solo and keratin filaments regulate epithelial tubule morphology. *Cell Structure and Function*, *43*(1), 95–105. https://doi.org/10.1247/csf.18010

Noh, K., Bach, D. H., Choi, H. J., Kim, M. S., Wu, S. Y., Pradeep, S., Ivan, C., Cho, M. S., Bayraktar, E., Rodriguez-Aguayo, C., Dasari, S. K., Stur, E., Mangala, L. S., Lopez-Berestein, G., & Sood, A. K. (2020). The hidden role of paxillin: localization to nucleus promotes tumor angiogenesis. *Oncogene*, 384–395. https://doi.org/10.1038/s41388-020-01517-3

Olayioye, M. A., Noll, B., & Hausser, A. (2019). Spatiotemporal control of intracellular membrane trafficking by rho gtpases. *Cells*, *8*(12), 1–23. https://doi.org/10.3390/cells8121478

Ortiz, M. A., Mikhailova, T., Li, X., Porter, B. A., Bah, A., & Kotula, L. (2021). Src family kinases, adaptor proteins and the actin cytoskeleton in epithelial-to-mesenchymal transition. *Cell Communication and Signaling*, *19*(1), 1–19. https://doi.org/10.1186/s12964-021-00750-x

Pasapera, A. M., Schneider, I. C., Rericha, E., Schlaepfer, D. D., & Waterman, C. M. (2010). Myosin II activity regulates vinculin recruitment to focal adhesions through FAK-mediated paxillin phosphorylation. *Journal of Cell Biology*, *188*(6), 877–890. https://doi.org/10.1083/jcb.200906012

Pascual-Vargas, P., Cooper, S., Sero, J., Bousgouni, V., Arias-Garcia, M., & Bakal, C. (2017). RNAi screens for Rho GTPase regulators of cell shape and YAP/TAZ localisation in triple negative breast cancer. *Scientific Data*, *4*, 1–13. https://doi.org/10.1038/sdata.2017.18

Piao, Y. J., Kim, H. S., Hwang, E. H., Woo, J., Zhang, M., & Moon, W. K. (2018). Breast cancer cell-derived exosomes and macrophage polarization are associated with lymph node metastasis. *Oncotarget*, *9*(7), 7398–7410. https://doi.org/10.18632/oncotarget.23238

Qin, R., Schmid, H., Münzberg, C., Maass, U., Krndija, D., Adler, G., Seufferlein, T., Liedert, A., Ignatius, A., Oswald, F., Eiseler, T., & von Wichert, G. (2015). Phosphorylation and turnover of paxillin in focal contacts is controlled by force and defines the dynamic state of the adhesion site. *Cytoskeleton*, *72*(2), 101–112. https://doi.org/10.1002/cm.21209

Ramirez-Rícardo, J., Leal-Orta, E., Martínez-Baeza, E., Ortiz-Mendoza, C., Breton-Mora, F., Herrera-Torres, A., Elizalde-Acosta, I., Cortes-Reynosa, P., Thompson-Bonilla, R., & Salazar, E. P. (2020). Circulating extracellular vesicles from patients with breast cancer enhance migration and invasion via a Src-dependent pathway in MDA-MB-231 breast cancer cells. *Molecular Medicine Reports*, *22*(3), 1932–1948. https://doi.org/10.3892/mmr.2020.11259

Reinecke, J., & Caplan, S. (2014). Endocytosis and the Src family of non-receptor tyrosine kinases. *Biomolecular Concepts*, *5*(2), 143–155. https://doi.org/10.1515/bmc-2014-0003

Ridley, A. J. (2011). Life at the leading edge. *Cell*, *145*(7), 1012–1022. https://doi.org/10.1016/j.cell.2011.06.010

Rodriguez, P. L., Sahay, S., Olabisi, O. O., & Whitehead, I. P. (2007). ROCK I-mediated activation of NF-κB by RhoB. *Cellular Signalling*, *19*(11), 2361–2369. https://doi.org/10.1016/j.cellsig.2007.07.021

Sachdev, S., Bu, Y., & Gelman, I. H. (2009). Paxillin-Y118 phosphorylation contributes to the control of Src-induced anchorage-independent growth by FAK and adhesion. *BMC Cancer*, *9*, 1–14. https://doi.org/10.1186/1471-2407-9-12

Samuelsson, M., Potrzebowska, K., Lehtonen, J., Beech, J. P., Skorova, E., Uronen-Hansson, H., & Svensson, L. (2017). RhoB controls the Rab11-mediated recycling and surface reappearance of LFA-1 in migrating T lymphocytes. *Science Signaling*, *10*(509). https://doi.org/10.1126/scisignal.aai8629

Sandilands, E., Cans, C., Fincham, V. J., Brunton, V. G., Mellor, H., Prendergast, G. C., Norman, J. C., Superti-Furga, G., & Frame, M. C. (2004). RhoB and actin polymerization coordinate Src activation with endosome-mediated delivery to the membrane. *Developmental Cell*, *7*(6), 855–869. https://doi.org/10.1016/j.devcel.2004.09.019

Sawayama, T., Nakashima, K., Ichimura, T., Sakai, R., & Uekita, T. (2019). Homophilic complex formation of CDCP1 via the extracellular CUB2 domain facilitates SFK activation and promotes cancer cell migration. *Oncology Reports*, *42*(4), 1507–1516. https://doi.org/10.3892/or.2019.7271

Seo, C. H., Furukawa, K., Montagne, K., Jeong, H., & Ushida, T. (2011). The effect of substrate microtopography on focal adhesion maturation and actin organization via the RhoA/ROCK pathway. *Biomaterials*, *32*(36), 9568–9575. https://doi.org/10.1016/j.biomaterials.2011.08.077

Shortrede, J. E., Uzair, I. D., Neira, F. J., Flamini, M. I., & Sanchez, A. M. (2016). Paxillin, a novel controller in the signaling of estrogen to FAK/N-WASP/Arp2/3 complex in breast cancer cells. *Molecular and Cellular Endocrinology*, *430*, 56–67. https://doi.org/10.1016/j.mce.2016.04.007

Simatou, A., Simatos, G., Goulielmaki, M., Spandidos, D. A., Baliou, S., & Zoumpourlis, V. (2020). Historical retrospective of the SRC oncogene and new perspectives. *Molecular and Clinical Oncology*, *13*(4), 1–10. https://doi.org/10.3892/mco.2020.2091

Singh, D. D., & Yadav, D. K. (2021). TNBC: Potential targeting of multiple receptors for a therapeutic breakthrough, nanomedicine and immunotherapy. *Biomedicines*, *9*(8), 1–26. https://doi.org/10.3390/biomedicines9080876

Sun, X., Wang, M., Wang, M., Yu, X., Guo, J., Sun, T., Li, X., Yao, L., Dong, H., & Xu, Y. (2020). Metabolic Reprogramming in Triple-Negative Breast Cancer. *Frontiers in Oncology*, *10*(March). https://doi.org/10.3389/fonc.2020.00428

Svensmark, J. H., & Brakebusch, C. (2019). Rho GTPases in cancer: friend or foe? *Oncogene*, *38*(50), 7447–7456. https://doi.org/10.1038/s41388-019-0963-7

Tanaka, K., Ito, Y., Kajiwara, K., Nada, S., & Okada, M. (2020). Ubiquitination of Src promotes its secretion via small extracellular vesicles. *Biochemical and Biophysical Research Communications*, *525*(1), 184–191. https://doi.org/10.1016/j.bbrc.2020.02.057

Theocharis, S., Kotta-Loizou, I., Giaginis, C., Alexandrou, P., Danas, E., Tsouroufl is, G., Tsoukalas, N., Coutts, R. H. A., Tasoulas, J., & Klijanienko, J. (2017). Expression and clinical significance of concomitant fak/src and p-paxillin in mobile tongue squamous cell carcinoma. *Anticancer Research*, *37*(3), 1313–1319. https://doi.org/10.21873/anticanres.11449

Tickner, J. A., Urquhart, A. J., Stephenson, S. A., Richard, D. J., & O'Byrne, K. J. (2014). Functions and therapeutic roles of exosomes in cancer. *Frontiers in Oncology*, *4 MAY*(May), 2–9. https://doi.org/10.3389/fonc.2014.00127

Tojkander, S., Gateva, G., & Lappalainen, P. (2012). Actin stress fibers - Assembly, dynamics and biological roles. *Journal of Cell Science*, *125*(8), 1855–1864. https://doi.org/10.1242/jcs.098087

Tokuraku, K., Kuragano, M., & Uyeda, T. Q. P. (2020). Long-range and directional allostery of actin filaments plays important roles in various cellular activities. *International Journal of Molecular Sciences*, *21*(9). https://doi.org/10.3390/ijms21093209

Tu, C., Ortega-Cava, C. F., Winograd, P., Stanton, M. J., Reddi, A. L., Dodge, I., Arya, R., Dimri, M., Clubb, R. J., Naramura, M., Wagner, K. U., Band, V., & Band, H. (2010). Endosomal-sorting complexes required for transport (ESCRT) pathway-dependent endosomal traffic regulates the localization of active Src at focal adhesions. *Proceedings of the National Academy of Sciences of the United States of America*, *107*(37), 16107–16112. https://doi.org/10.1073/pnas.1009471107

Turner, C. E. (2000). Paxillin and focal adhesion signalling. *Nature Cell Biology*, *2*(12), 231–236. https://doi.org/10.1038/35046659

Ullah, F. (2019). Breast cancer: current perspectives on the disease status. In A.Ahmad (Ed.), *Breast cancer metastasis and drug resistance* (pp 51-64). Switzerland: Springer.

Vagia, E., Mahalingam, D., & Cristofanilli, M. (2020). The landscape of targeted therapies in TNBC. *Cancers*, *12*(4). https://doi.org/10.3390/cancers12040916

Vega, F. M., Colomba, A., Reymond, N., Thomas, M., & Ridley, A. J. (2012). RhoB regulates cell migration through altered focal adhesion dynamics. *Open Biology*, *2*(MAY). https://doi.org/10.1098/rsob.120076

Wallar, B. J., DeWard, A. D., Resau, J. H., & Alberts, A. S. (2007). RhoB and the mammalian Diaphanous-related formin mDia2 in endosome trafficking. *Experimental Cell Research*, *313*(3), 560–571. https://doi.org/10.1016/j.yexcr.2006.10.033

Wang, W. Y., Pearson, A. T., Kutys, M. L., Choi, C. K., Wozniak, M. A., Baker, B. M., & Chen, C. S. (2018). Extracellular matrix alignment dictates the organization of focal adhesions and directs uniaxial cell migration. *APL Bioengineering*, *2*(4). https://doi.org/10.1063/1.5052239

Warner, H., Wilson, B. J., & Caswell, P. T. (2019). Control of adhesion and protrusion in cell migration by Rho GTPases. *Current Opinion in Cell Biology*, *56*, 64–70. https://doi.org/10.1016/j.ceb.2018.09.003

Weigelt, B., Peterse, J. L., & Van't Veer, L. J. (2005). Breast cancer metastasis: Markers and models. *Nature Reviews Cancer*, *5*(8), 591–602. https://doi.org/10.1038/nrc1670

Woods, A. J., Kantidakis, T., Sabe, H., Critchley, D. R., & Norman, J. C. (2005). Interaction of Paxillin with Poly(A)-Binding Protein 1 and Its Role in Focal Adhesion Turnover and Cell Migration. *Molecular and Cellular Biology*, *25*(9), 3763–3773. https://doi.org/10.1128/mcb.25.9.3763-3773.2005

World Health Organization (2021, March 26). *Breast cancer*. WHO. https://www.who.int/news-room/fact-sheets/detail/breast-cancer

Wu, J. C., Chen, Y. C., Kuo, C. T., Yu, H. W., Chen, Y. Q., Chiou, A., & Kuo, J. C. (2015). Focal adhesion kinase-dependent focal adhesion recruitment of SH2 domains directs SRC into focal adhesions to regulate cell adhesion and migration. *Scientific Reports*, *5*(December), 1–13. https://doi.org/10.1038/srep18476

Wu, Y., Zhang, K., Seong, J., Fan, J., Chien, S., Wang, Y., & Lu, S. (2016). In-situ coupling between kinase activities and protein dynamics within single focal adhesions. *Scientific Reports*, *6*(February), 1–13. https://doi.org/10.1038/srep29377

Xie, Y. G., Yu, Y., Hou, L. K., Wang, X., Zhang, B., & Cao, X. C. (2016). FYN promotes breast cancer progression through epithelial-mesenchymal transition. *Oncology Reports*, *36*(2), 1000–1006. https://doi.org/10.3892/or.2016.4894

Xue, Q., Varady, S. R. S., Alaka'i Waddell, T. Q., Carrington, J., & Roh-Johnson, M. (2022). Focal adhesion-based cell migration is differentially regulated in vivo versus in vitro by Paxillin phosphorylation. *BioRxiv*, 2022.03.02.482703. https://doi.org/10.1101/2022.03.02.482703

Yodoi, R., Tamba, S., Morimoto, K., Segi-Nishida, E., Nishihara, M., Ichikawa, A., Narumiya, S., & Sugimoto, Y. (2009). RhoA/Rho kinase signaling in the cumulus mediates extracellular matrix assembly. *Endocrinology*, *150*(7), 3345–3352. https://doi.org/10.1210/en.2008-1449

Zaidel-Bar, R., Milo, R., Kam, Z., & Geiger, B. (2007). A paxillin tyrosine phosphorylation switch regulates the assembly and form of cell-matrix adhesions. *Journal of Cell Science*, *120*(1), 137–148. https://doi.org/10.1242/jcs.03314

Zeichner, S. B., Terawaki, H., & Gogineni, K. (2016). A review of systemic treatment in metastatic triple-negative breast cancer. *Breast Cancer: Basic and Clinical Research*, *10*, 25–36. https://doi.org/10.4137/BCBCr.s32783

Zhang, C., Wang, H. J., Bao, Q. C., Wang, L., Guo, T. K., Chen, W. L., Xu, L. L., Zhou, H. S., Bian, J. L., Yang, Y. R., Sun, H. P., Xu, X. L., & You, Q. D. (2016). NRF2 promotes breast cancer cell proliferation and metastasis by increasing RhoA/ROCK pathway signal transduction. *Oncotarget*, *7*(45), 73593–73606. https://doi.org/10.18632/oncotarget.12435